AR-008-582

DSTO-RR-0010

Electrical Performance Characterisation of Single-Shot Switches in High Speed, High Voltage and High Current Applications

Michael Podlesak

DEPARTMENT ◆ OF DEFENCE
DEFENCE SCIENCE AND TECHNOLOGY ORGANISATION

Electrical Performance Characterisation of Single-Shot Switches in High Speed, High Voltage and High Current Applications

Michael Podlesak

Aeronautical and Maritime Research Laboratory

ABSTRACT

Research Report

The electrical performance characteristics of single-shot closing switches for slapper detonator applications were measured via the discharge of a low impedance transmission line. The switch performance, characterised by its time-dependent resistance behaviour, could not be assessed via the more conventional methods of measurement because of high bandwidth requirements at comparatively high levels of voltage and current. Hence, an alternative technique based on a transmission line discharge was devised in which the time-dependent resistance of the switch can be determined from the measured current waveform of the switch, the initial open circuit voltage and the transmission line parameters only. Under certain conditions a simple lossless transmission line formula is sufficient for the calculation of the switch resistance waveform. However, if the transmission line losses cannot be neglected, a correction can be readily implemented through numerical signal processing. The bandwidth of this technique is limited to the bandwidth of the switch current measurement only, which proved to be particularly useful for the measurement of switches for slapper detonator applications where inductive pick-up noise in the switch voltage waveform is large and where high voltage probes of sufficiently high bandwidth are not readily available. In this report, both numerically simulated and experimental examples are given, together with the method of calculation of switch resistance which takes into account practical transmission line losses. It was found that best results are obtained if the magnitude of the switch resistance is of a similar order as the characteristic impedance of the transmission line, or higher.

Approved for public release

DSTO-RR-0010

DEPARTMENT OF DEFENCE

DEFENCE SCIENCE AND TECHNOLOGY ORGANISATION

Published by

DSTO Aeronautical and Maritime Research Laboratory
GPO Box 4331
Melbourne Victoria 3001

Telephone: (03) 626 8111
Fax: (03) 626 8999

AR No. 008-582
August 1994

APPROVED FOR PUBLIC RELEASE

Author

Michael Podlesak

Michael Podlesak obtained BSc(Hons) in Physics in 1980 and PhD in Physics, Acoustics, in 1986, at La Trobe University. After one year of postdoctoral work in acoustics, and one year of physics teaching and research in the area of optical fibre application to sensing with the Department of Applied Physics at Footscray Institute of Technology, Dr Podlesak joined the Explosives Ordnance Division, MRL in 1988, to carry out experimental work in slapper detonator research and study shock wave phenomena in inert and energetic materials using electrically based launching methods. He is currently working in the Ship Structures and Materials Division on problems related to control of acoustic signatures of naval vessels.

Contents

Electrical Performance Characterisation of Single-Shot Switches in High Speed, High Voltage and High Current Applications

1. Introduction

In pulsed power applications, the knowledge of the electrical performance of fast closing switches is crucial to maximising the system efficiency. For example, fast flying plates may be generated by electrically exploding thin metal foils via the discharge of a high voltage capacitor [1-6]. The energy efficiency of this technique and other similar processes relies on the nature of the load and system parameters [7], among which the switch plays an important role. Once the time-dependent resistance characteristic of a switch is known, it can be incorporated into the total system model which is then optimised for maximum efficiency.

1.1 Limitations of the Classic Approach to Resistance Measurement

Traditionally, time-dependent switch resistance $r(t)$ is determined from the measurement of switch current $i(t)$ and voltage $v(t)$ according to Ohm's law:

$$r(t) = v(t) / i(t). \qquad (1)$$

Generally, the current measurement can be performed by using electrical transducers such as a current viewing resistor (CVR), current transformer (CT) or a Rogowski coil [8,9]. The measurement of voltage across the switch is usually performed with either a commercial high impedance voltage probe or by a custom-designed high impedance voltage divider network.

In pulsed power applications, currents are frequently easier to measure than voltages, particularly when high rates of current change

are involved, e.g., where $di(t)/dt$ magnitudes are of the order of 10^{11} A/s or larger. Also, at radio frequencies, it is difficult to design a voltage probe which has both high voltage rating and high signal bandwidth. In most applications, satisfactory voltage probes may be found to meet the specific requirements, but in the measurement of voltage across fast-acting switches involving high voltages and currents, conflicting performance demands prevent accurate measurements.

Two major limitations exist. The first refers to the mutual inductance effect between the voltage probe and the circuit element under test [10]. In many instances, it is impossible to completely eliminate the inductive pick-up loop formed by the probe's input section and the switch under test. Thus, even with an inductive coupling of 1 nH or less, the induced voltages can be of the order of 100 V for $di(t)/dt \geq 10^{11}$ A/s. While inductive noise cancelling strategies exist [11], their accuracy is limited because of phase and amplitude inaccuracies at high frequencies as well as the problem of maintaining constant inductive coupling between consecutive experiments.

The second limitation refers to the conflicting requirements of high voltage, high input impedance and high signal bandwidth. Passive probes are usually based on a resistive divider network with capacitive compensation and are limited in their bandwidth in proportion to the reciprocal product of their input resistance and capacitance. Also, at high frequencies, the divider network becomes predominantly capacitive rather than resistive and thereby lowers the probe's input impedance with increasing signal frequency and hence reduces the probe's voltage rating through increased current flow. Commercial active probes display very high bandwidth and input impedance, but are limited to operation at low voltages.

1.2 *Switch Resistance Measurement via a Transmission Line Discharge Technique*

The method of switch resistance measurement proposed in this report eliminates the need for the dynamic measurement of switch voltage. In principle, the method consists of placing the switch at one end of a charged uniform transmission line, as portrayed in Fig. 1, which is then discharged through the switch after closure. The current is monitored near the switch and is measured for the duration of at least one journey of the current wave along the full length of the transmission line, but no more than the full to-and-fro journey. The theory for a semi-infinite uniform transmission line in Section 2 shows that the time-dependent resistance of the switch, which is assumed to present a purely resistive load[1], can be expressed in terms of the switch current, initial voltage and the distributed parameters of a transmission line ,

[1]In a capacitive discharge system, the discharge current is limited by the system resistance and the reactive impedance due to the system inductance. The switch contributes to the system resistance and inductance, but the switches used in our applications were specifically designed to be of low inductance by utilising stripline geometry.

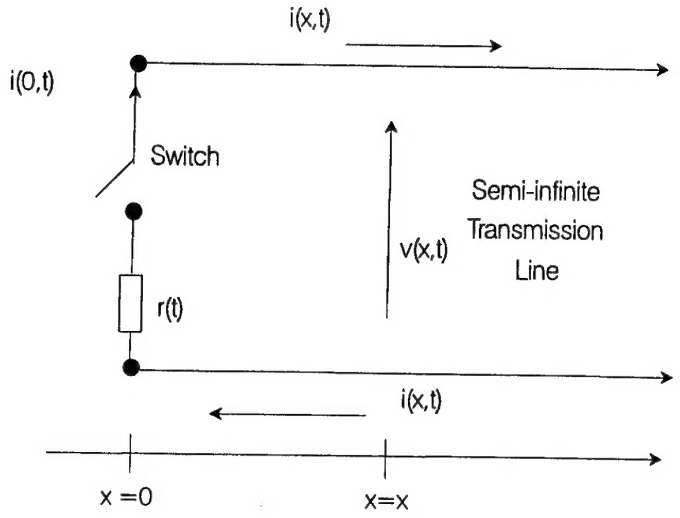

Figure 1: *Schematic representation of a switch with time-dependent resistance r(t), connected to a semi-infinite transmission line. i(0,t) represents the switch current and i(x,t) the transmission line current at some arbitrary point* $x \geq 0$.

namely inductance, capacitance and resistance per unit length. Thus the bandwidth of the resistance waveform is limited by the bandwidth of the current measurement only.

The method is very simple in cases where transmission line losses can be neglected and has been used in studies of exploding wires [12]. However, if the line losses cannot be neglected, a number of correction terms can be applied by further numerical processing of the data. The theory required for the corrections is developed in Section 2. Section 3 outlines the basic experimental technique and Section 4 deals with the experimental measurement aspects as well as numerical simulations of a realistic transmission line used to verify and elucidate various features of the transmission-line based measurement technique. Section 5 discusses some of the advantages and limitations of the new technique.

2. *Theoretical Transmission Line Derivations*

Consider the case of a one-dimensional, uniform, semi-infinite, electrically conducting transmission line, charged to a voltage V_0 at time $t \leq 0$. Fig. 1 shows schematically the transmission line which is open ended at $x \to \infty$ and terminated by a switch at $x = 0$, whose time-dependent resistance is denoted by $r(t)$. The voltage and current along the transmission line are denoted by $v(x,t)$ and $i(x,t)$, respectively. The boundary and initial conditions are: $v(0,t) = -r(t)\, i(0,t)$ and when $t \leq 0$ $i(x,t) = 0$ and $v(x,t) = V_0$. Also, $\partial v(x,0)/\partial x = 0$ and $\partial i(x,0)/\partial x = 0$.

2.1 *General Equations for a Uniform One-Dimensional Transmission Line*

While the basic derivations for a uniform one-dimensional transmission line are well known, we set them out here for reference in order to study their particular application to the switch resistance measurement problem. The transmission line parameters constitute the usual distributed inductance L, capacitance C, resistance R and conductance G (see for example References 13-15), which are assumed constant over the frequency range of our measurements. Our experimental work has shown this assumption to hold quite well within our terms of reference, however, the effect of variation of L, C, R and G with frequency is explained in Section 5.5. The fundamental equations governing wave propagation along a uniform linear transmission line are [13]:

$$L\partial i(x,t) / \partial t + Ri(x,t) = -\partial v(x,t) / \partial x \qquad (2)$$

$$C\partial v(x,t) / \partial t + Gi(x,t) = -\partial i(x,t) / \partial x \qquad (3)$$

Eqs. (2)-(3) are simultaneous partial differential equations with independent variables x and t. These can be solved with the aid of Laplace transformations (see for example References 13, 16 and 17) with the boundary conditions applied either in the transformed space or in the time domain. The transformed Eqs. (2) and (3) are

$$(Ls + R)I(x,s) = -\partial V(x,s) / \partial x + Li(x,0) \qquad (4)$$

$$(Cs + G)V(x,s) = -\partial I(x,s) / \partial x + Cv(x,0) \qquad (5)$$

where the transformed current and voltage are $I(x,s)$ and $V(x,s)$ and s represents the usual complex variable in the Laplace transformed space. Since s is not a function of x and there are no derivatives with respect to s, Eqs. (4) and (5) can be treated as a pair of simultaneous ordinary differential equations. We obtain [13]

$$\partial^2 I(x,s) / \partial x^2 - (Ls + R)(Cs + G)I(x,s) = C\partial v(x,0) / \partial x - L(Cs + G)i(x,0) \qquad (6)$$

$$\partial^2 V(x,s)/\partial x^2 - (Ls+R)(Cs+G)V(x,s) = L\partial i(x,0)/\partial x - C(Ls+R)v(x,0) \quad (7)$$

By letting $n = \sqrt{(Ls+R)(Cs+G)}$, sometimes called the propagation constant, the complementary functions of the solutions to Eqs. (6) and (7) are of the form

$$I(x,s) = A_1(s)e^{-nx} + B_1(s)e^{nx} \quad (8)$$

$$V(x,s) = A_2(s)e^{-nx} + B_2(s)e^{nx}, \quad (9)$$

where $A(s)$ and $B(s)$ are independent of x, but are arbitrary functions of s to be determined from the initial and boundary conditions of the problem.

2.2 *Application of Initial and Boundary Conditions*

2.2.1 *Case of $R > 0$ and $G > 0$*

Since $I(x,s)$ and $V(x,s)$ must be finite for $x \to \infty$, then coefficients $B_1(s) = B_2(s) = 0$. Also, since at $t \le 0$, $v(x,t) = V_0$, then Eq. (7) is not homogeneous and we need to add the particular solution to the complementary solution given by Eq. (9). Assume a particular solution of the form $V(x,s) = K(s)$. Then $K(s) = V_0/(s+G/C)$. Thus Eqs. (8) and (9) take on the form of

$$I(x,s) = A_1(s)e^{-nx} \quad (10)$$

$$V(x,s) = A_2(s)e^{-nx} + V_0/(s+G/C), \quad (11)$$

respectively. Substituting Eq. (11) into Eq. (4) yields

$$I(x,s) = nA_2(s)e^{-nx}/(Ls+R), \quad (12)$$

since $i(x,0) = 0$ at $t \le 0$. By comparing coefficients of Eqs. (10) and (12), we obtain

$$A_2 = A_1(s)e^{-nx}(Ls+R)/n. \quad (13)$$

Setting $A(s) = A_1(s)$, Eqs. (10) and (11) may be rewritten as

$$I(x,s) = A(s)e^{-nx} \quad (14)$$

$$V(x,s) = A(s)(Ls+R)e^{-nx}/n + V_0/(s+G/C) \quad (15)$$

It is useful at this stage to simplify the problem by considering the current and voltage at the switch end of the line, i.e., at $x = 0$. Then Eq. (14) reduces to

$$I(0,s) = A(s), \tag{16}$$

which is substituted into Eq. (15) to obtain

$$V(0,s) = I(0,s)(Ls+R)/n + V_0/(s+G/C)\,. \tag{17}$$

For convenience, define $\delta = R/L$, $\sigma = G/C$ and $Z_0 = \sqrt{L/C}$ (commonly known as the characteristic impedance of the transmission line), so that with $n = \sqrt{(Ls+R)(Cs+G)} = \sqrt{LC(s+\delta)(s+\sigma)}$ Eq. (17) becomes

$$V(0,s) = Z_0 I(0,s)\sqrt{1+\frac{(\delta-\sigma)}{s}\left[1-\frac{\sigma}{s}+\left(\frac{\sigma}{s}\right)^2-\left(\frac{\sigma}{s}\right)^3+\ldots\right]}+\frac{V_0}{(s+\sigma)}. \tag{18}$$

Provided that second and higher order terms of (σ/s) are neglected (i.e., $|\sigma/s| << 1$, which in practice can be generally satisfied [14], then Eq. (18) reduces to

$$V(0,s) = Z_0 I(0,s)\sqrt{1+\frac{(\delta-\sigma)}{s}}+\frac{V_0}{(s+\sigma)}. \tag{19}$$

For sufficiently high signal frequencies, the term $\sqrt{1+(\delta-\sigma)/s}$ may be expanded binomially, as long as $|(\delta-\sigma)/s| < 1$. Defining $(\delta-\sigma) = \gamma$, we express Eq. (19) as

$$V(0,s) = Z_0 I(0,s)\left[1+\frac{1}{2}\left(\frac{\gamma}{s}\right)-\frac{1}{8}\left(\frac{\gamma}{s}\right)^2+\frac{1}{16}\left(\frac{\gamma}{s}\right)^3-\ldots \right.$$
$$\left.\ldots+\left(\frac{\gamma}{s}\right)^k\frac{(1/2)!}{(1/2-k)!k!}\ldots\right]+\frac{V_0}{(s+\sigma)}, \tag{20}$$

where k is a non-negative integer and the co-efficients of $(\gamma/s)^k$ are the binomial coefficients ${}^{1/2}C_k = (1/2)!/[(1/2-k)!k!] =$ $\Gamma(3/2)/[\Gamma(3/2-k)\Gamma(k+1)]$, following the standard definition of the mathematical Gamma function.

Since the switch resistance function $r(t)$ is not known, except that $r(t)$ and its time derivatives are continuous, it is not possible to explicitly transform the boundary condition $v(0,t) = r(t)i(0,t)$. Therefore, we apply the boundary condition in the time domain to the inverse transform [16,17] of Eq. (20), which is of the form:

$$v(0,t) = Z_0\left[i(0,t) + \left(\frac{\gamma}{2}\right)\int_{t=0}^{t} i(0,t)dt - \left(\frac{\gamma^2}{8}\right)\int_{t=0}^{t}\int_{t_1=0}^{t_1} i(0,t)dt_1 dt + \ldots \right.$$

$$\left. \ldots + \frac{\gamma^k (1/2)!}{(1/2-k)!k!}\int_{t=0}^{t}\int_{t_k=0}^{t_k}\cdots\int_{t_1=0}^{t_1} i(0,t)dt_1 \ldots dt_k dt + \ldots \right] + V_0 e^{-\sigma t}, \qquad (21)$$

where k is a positive integer. Thus

$$r(t) = -\frac{Z_0}{i(0,t)}\left[i(0,t) + \left(\frac{\gamma}{2}\right)\int_{t=0}^{t} i(0,t)dt - \left(\frac{\gamma^2}{8}\right)\int_{t=0}^{t}\int_{t_1=0}^{t_1} i(0,t)dt_1 dt + \ldots \right.$$

$$\left. \ldots + \frac{\gamma^k (1/2)!}{(1/2-k)!k!}\int_{t=0}^{t}\int_{t_k=0}^{t_k}\cdots\int_{t_1=0}^{t_1} i(0,t)dt_1 \ldots dt_k dt + \ldots \right] - \frac{V_0 e^{-\sigma t}}{i(0,t)}. \qquad (22)$$

Note that Eq.(22) holds only for values of G small enough so that the assumption $|\sigma / s| << 1$ made in Eq.(19) is not violated.

2.2.2 *Case of R > 0 and G = 0*

It should be noted that in practice the value of G, normally associated with dielectric losses, varies with frequency. This would render Eq. (22) invalid, as would skin effect induced variations in R (refer to Section 5.5). However, according to Chipman [14] the value of G increases approximately linearly with angular frequency ω (here, the imaginary component of s), but the ratio $G/\omega C = \sigma/\omega$ is always small and generally approaches a small constant fraction at very high frequencies. Therefore, the G term is neglected in most applications, including our own. Setting $G = 0$ implies $\sigma = 0$ and γ becomes $\delta = R/L$, and Eq. (22) may be further simplified to obtain

$$r(t) = -\frac{Z_0}{i(0,t)}\left[i(0,t) + \left(\frac{\delta}{2}\right)\int_{t=0}^{t} i(0,t)dt - \left(\frac{\delta^2}{8}\right)\int_{t=0}^{t}\int_{t_1=0}^{t_1} i(0,t)dt_1 dt + \ldots \right.$$

$$\left. \ldots + \frac{\delta^k (1/2)!}{(1/2-k)!k!}\int_{t=0}^{t}\int_{t_k=0}^{t_k}\cdots\int_{t_1=0}^{t_1} i(0,t)dt_1 \ldots dt_k dt + \ldots \right] - \frac{V_0}{i(0,t)}. \qquad (23)$$

With the aid of numerical processing packages, Eq. (23) is amenable to evaluation of $r(t)$ from experimentally obtained waveforms of $i(0,t)$.

Before closing Section 2, we set out some of the simpler cases arising from Eq. (23), which are relevant to understanding certain experimental results.

2.2.3 *Case of $R = 0$ and $G = 0$*

If $R = 0$, then $\delta = 0$ and Eq. (23) reduces to

$$r(t) = -Z_0 - V_0 / i(0,t) \tag{24}$$

This simple form is applicable either to very low loss lines, or for sufficiently short signal duration, where the effect of signal decay due to resistive dissipation in the line is negligible. We note in passing that a similar equation applies for the condition met in Heaviside's distortionless line [13], i.e., $R > 0$, $G > 0$ and $R / L = G / C$. This sets $\gamma = 0$ in Eq. (22) and reduces it to Eq. (24) with V_0 multiplied by a simple exponential decay term $e^{-\sigma t} = e^{-G/C}$.

2.2.4 *Case of $R > 0$, $G = 0$, and Constant Switch Resistance $r(t) = r_0$ for $t \geq 0$*

In the case of constant switch resistance $r(t) = r_0$, for $t \geq 0$, the boundary condition $v(0,t) = -r(t)i(0,t)$ transforms easily into $V(0,s) = -r_0 I(0,s)$, which is substituted into Eq. (19). Setting $\sigma = 0$ for the case of $G = 0$, we obtain

$$-r_0 I(0,s) = Z_0 I(0,s)\sqrt{1 + (\delta/s)} + V_0/s \tag{25}$$

Considering the simpler case of $|\delta / s| << 1$, so that $\sqrt{1 + (\delta / s)} \approx 1 + \delta/(2s)$, Eq. (25) becomes

$$I(0,s) = -\frac{V_0}{(r_0 + Z_0)\left[s + \dfrac{Z_0(\delta/2)}{(r_0 + Z_0)}\right]} \tag{26}$$

which, when transformed into the time domain, yields

$$i(0,t) = -\frac{V_0}{(r_0 + Z_0)} e^{\left(-t\frac{Z_0(\delta/2)}{(r_0+Z_0)}\right)}. \tag{27}$$

In terms of the limiting assumptions, Eq.(27) is valid within $0 \leq t < (1/\delta)$, assuming $|\delta / s| \leq 0.1$. Clearly, the decay rate of the current waveform depends not only on the value of δ, but also the ratio of $Z_0 / (r_0 + Z_0)$. However, for $r_0 << Z_0$, the decay rate of the current waveform is practically independent of the switch resistance r_0 and Eq. (27) approximates the simple form of

$$r_0 \cong -Z_0 - \frac{V_0}{i(0,t)} e^{-\left(\frac{\delta}{2}t\right)}. \tag{28}$$

Also, for sufficiently large values of r_0, the decay coefficient $Z_0(\delta/2)/(r_0+Z_0)$ may become negligible so that Eq. (28) reduces to the simplest form given by Eq. (24). For a less than a 5% error, the limit for the duration of the switch current is $0 \le t < (0.1r_0)/(Z_0\delta)$.

3. *Experimental Technique and Apparatus*

The experimental technique was designed around specific evaluation criteria for a fast, high current, high voltage switch intended for slapper detonator applications. The particular application required a total switch operation time of 200 ns or less, closure time of about 20 ns or less, and current magnitudes of the order of 2 kA at 2 kV charge voltage. The desired minimum signal bandwidth spanned 5 - 200 MHz, representing a maximum rise times of the order of 1 ns. Such bandwidth corresponds to current rates of change between 10^{10} and 10^{12} A/s, which can give rise to significant levels of inductive pick-up noise in the conventional voltage measurements, as mentioned in Section 1.1. To meet the above current and voltage requirements, a low impedance parallel-strip transmission line was built according to the description in Appendix B.

A schematic view of the basic experimental set-up is given in Fig. 2. It shows one end of the strip line connected to a clamping type current viewing resistor[2] and a switch, and the other end of the line connected to a high voltage dc power supply. The charge voltage V_0 was monitored at the voltage supply end via a Radio Spares 40 kV, 1 GΩ, 1000:1 dc voltage probe.

Some measurements included a 100:1 Tektronix P6009 voltage probe, with 10 MΩ input impedance, 1.5 kV dc maximum voltage rating and bandwidth of 0 - 120 MHz. These were performed on switches with relatively low values of di(0,t)/dt and were used primarily for the calibration of transmission line parameters, as explained in Section 4.2.

The current and voltage waveforms were recorded either via a Tektronix DSA 602 digital signal analyser or a Tektronix 2440 digitizing oscilloscope. The DSA 602 was run at a digitizing rate of 10^9 samples/s with signal amplifier bandwidth of 0 - 1 GHz. The 2440 oscilloscope was run at maximum rate of 5×10^8 samples/s with signal amplifier bandwidth of 0 - 200 MHz. The analog-to-digital converters in both machines had 8 bit resolution. The data were collected on a personal computer via an IEEE-488 general purpose interface bus with the aid of a communication and signal processing software package [18]. The

[2]Current viewing resistors employed were produced by T & M Research Products, Albuquerque, New Mexico, USA. The model W-2-0025C-2FC has nominal insertion resistance of 2.5 mΩ, 2 ns risetime and bandwidth 0 - 200 MHz. The model W-1-01C-2FC has nominal insertion resistance of 10 mΩ, 0.45 ns risetime and bandwidth 0 - 800 MHz. Low inductance is claimed, but not specified.

signal processing software was used to process the acquired waveforms to calculate r(t) according to either Eq. (1) or Eq. (23).

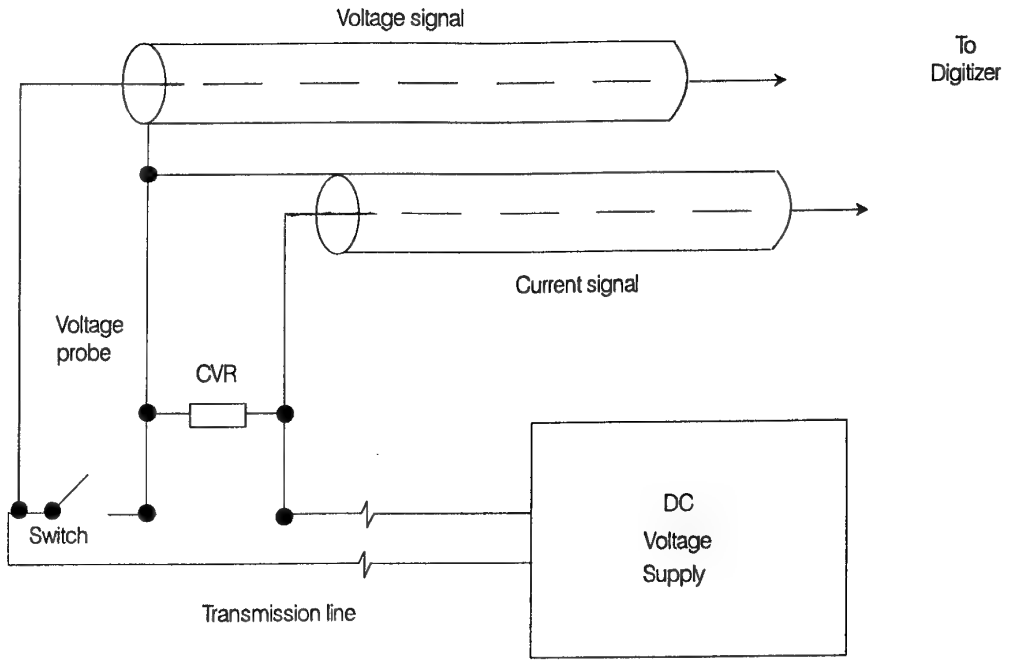

Figure 2: *Basic set-up of the apparatus for the transmission-line based switch resistance measurement. The switch voltage measurement is performed only during calibration of the transmission line parameters. The current detector shown is a current viewing resistor (CVR).*

4. Experiments

Both simulated and practical switch current and voltage waveforms were obtained. The simulated waveforms, based on the transmission line model outlined in Appendix A, were used to verify the efficacy of the switch resistance calculations according to Eq. (23) and to illustrate the sensitivity of the solution to variations in transmission line parameters. Practical switch examples include an explosive actuated (EA) switch, a triggered vacuum gap (TVG) switch and a simple atmospheric gap breakdown (AGB) switch. The AGB switch experiments were used in calibrations of the transmission line parameters *L*, *C* and *R*.

4.1 Numerical Simulations

The numerical code for the transmission line model in Appendix A was written in FORTRAN computer programming language, using double precision mode of calculation. Switch current, voltage and resistance records of 1 μs duration were generated. The transmission line parameters were chosen to closely represent those of the actual strip line. The switch resistance model was based on a simple representation of some experimental switch measurements, comprising a two step exponential decay followed by a constant final value.

An example of a simulated switch current and voltage waveform is shown in Figs. 3(a) and 3(b), respectively, using a transmission line of length ℓ = 33.0 m, divided into 1000 discrete elements with lumped parameters L = 165.0 pH, C = 273.9 pF, R = 1.049 mΩ and G = 0.0 Ω^{-1}. The initial line voltage was V_0 = 1.0 V and the termination resistance at the other end of the line was set to $R_t = 1.0 \times 10^6 \Omega$, simulating an open circuit condition. The time step between each iteration was $\Delta t = 5.0 \times 10^{-11}$s, and the switch resistance waveform $r(t)$, shown in Fig. 3(c), was defined as:

$$r(t) = \begin{cases} 1.8e^{-1.28\times10^8 t} \text{ for } 0 \le t \le 1.0\times10^{-8} \\ 1.0772e^{-7.6753\times10^7 t} \text{ for } 1.0\times10^{-8} \le t \le 4.0\times10^{-8} \\ 0.05 \text{ for } t \ge 4.0\times10^{-8} \end{cases}$$

In the first exponential decay regime, the switch resistance waveform begins at, or below, the maximum value allowable by the model (see Appendix A) and drops to 0.5 Ω after 10 ns. In the second decay regime, the switch resistance drops from 0.5 Ω to 0.05 Ω within 30 ns and thereafter remains at a constant value of 0.05 Ω. The plotting frequency in Figs. 3(a) - 3(c) is one point per nanosecond.

Next, we illustrate the efficacy of the transmission line method by calculating the switch resistance waveform according Eq. (23), using the data from the simulated current waveform in Fig. 3(a) as input, and the resistance data in Fig. 3(c) as control. We show in Fig. 4 successive term-by-term approximations of the switch resistance superposed over the control curve (Fig. 3(c)) depicted by the dashed line. The symbols T0, T1, ..., T6 refer to the number of integration terms in Eq. (23) used to successively approximate the switch resistance waveform. The curve T7, not shown, coincides with the control curve over the displayed 400 ns time interval. Using this particular example it is evident that for

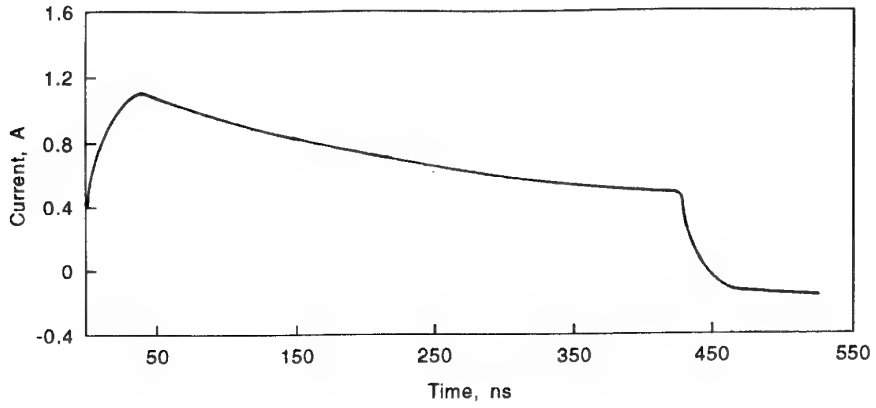

(a)

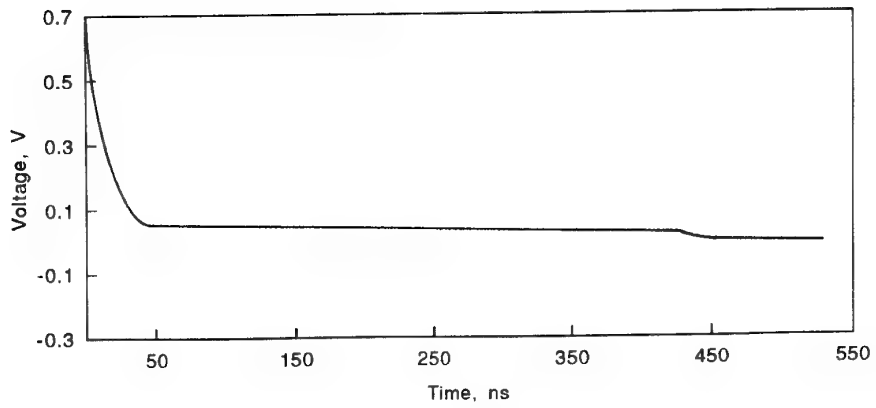

(b)

Figure 3: *Output waveforms from numerically simulated transmission line experiment. (a) shows switch current waveform i(0,t), (b) the switch voltage waveform v(0,t), and (c) the switch resistance waveform r(t).*

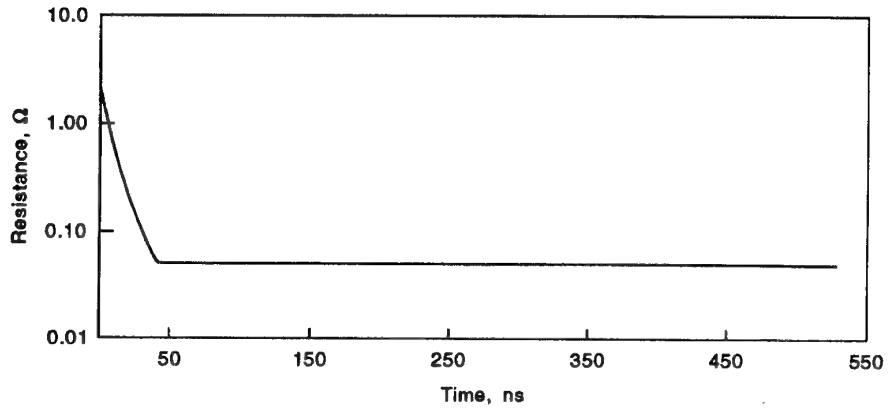

(c)

Figure 3: *Output waveforms from numerically simulated transmission line experiment. (a) shows switch current waveform i(0,t), (b) the switch voltage waveform v(0,t), and (c) the switch resistance waveform r(t).*

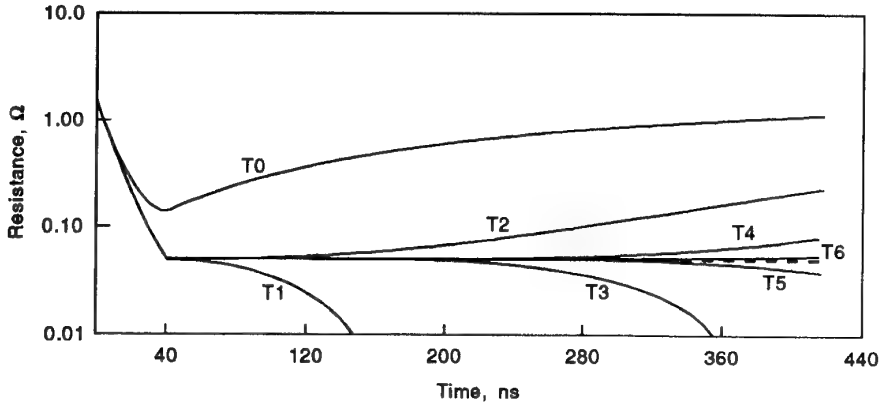

Figure 4: *Progressive approximations (solid lines) to the switch resistance waveform (dashed line) by evaluating an increasing number of integration terms in Eq. (23). T0, T1, T2, ... , T6 denote the number of integration terms used.*

shorter switch function times fewer terms would be required to calculate the switch resistance waveform within a specified level of accuracy. This characteristic is due to the integration terms which contribute increasingly with increasing time. For instance, a switch function time of 100 ns may require only two integration terms.

4.2 *Experimental Calibration of Transmission Line Parameters*

The strip line design, given in Appendix B, contains only nominal information with regard to transmission line parameters L, C and R. The level of accuracy provided by this type of information is generally inadequate for switch resistance calculations, where the switch resistance is of the order of the transmission line's characteristic impedance, or less. Further complications arise if the measurement duration is long enough for the line's resistive losses to become important, i.e., when Eq.(24) based on the lossless transmission line derivation no longer provides sufficiently accurate switch resistance waveforms.

Increased accuracy of the transmission line parameters may be achieved through calibration experiments based on the comparison of resistance waveforms obtained through Eqs. (1) and (23). The calibration experiments are performed under less demanding conditions, where reasonably accurate conventional voltage measurements across the switch can be made. Provided the signal propagation velocity c is known (see Appendix B), then only parametric adjustments of L and R are required to obtain a unique set of values for which the resistance waveforms according to Eqs. (1) and (23) are matched. [3]

The effectiveness of this calibration method is illustrated via the numerically simulated switch example. Firstly, consider Eq. (23) which uses transmission line parameters L, C and R. For high frequencies, the reactive impedances of the line dominate and the parameters L and C are simply coupled through $Z_0 = \sqrt{L/C}$ as well as the signal propagation velocity $c = 1/\sqrt{LC}$. From a practical viewpoint, this is of considerable significance since c is relatively easy to measure and therefore C may be replaced by $1/(Lc^2)$. Thus only L and R remain to be calibrated. The effect of varying L and R is demonstrated in Fig. 5, which shows the modelled switch resistance (solid line) calculated via Eq. (23), using the first seven integration terms. Variation of $L = 5.0 \pm 0.2$ nH/m causes mainly an offset of $\approx 0.03\,\Omega$, illustrated by the fine dashed curves. Variation of R, on the other hand, affects mainly the decay factor of the resistance waveform, with the coarse dashed curves representing variations of $R = 0.0318 \pm 0.0010\ \Omega/\text{m}$. The broad effects of these variations on the solution of Eq. (23) are more easily

[3] This calibration technique can be applied only to comparatively smooth switching waveforms, where the inductive pick-up noise in the conventional switch voltage measurement is minimal. Also, the voltages need to be low enough to allow for the use of voltage probes with sufficiently high bandwidth. Such limitations imposed on the transmission line calibrations are not unreasonable since the basic line parameters are expected to remain constant over a wide range of currents and voltages.

understood through the constant-closure-resistance case according to Eq. (28).

Eq. (28) contains a constant offset factor $Z_0 = (L / C)^{1/2}$, showing a strong dependence on L. While L is also contained in the damping term $\delta = R / L$ and affects the decay rate of the $i(0,t)$ waveform, the offset effect appears to be the more marked one. Variations in R bear a direct influence on the decay rate of the $i(0,t)$ waveform and tend to have a

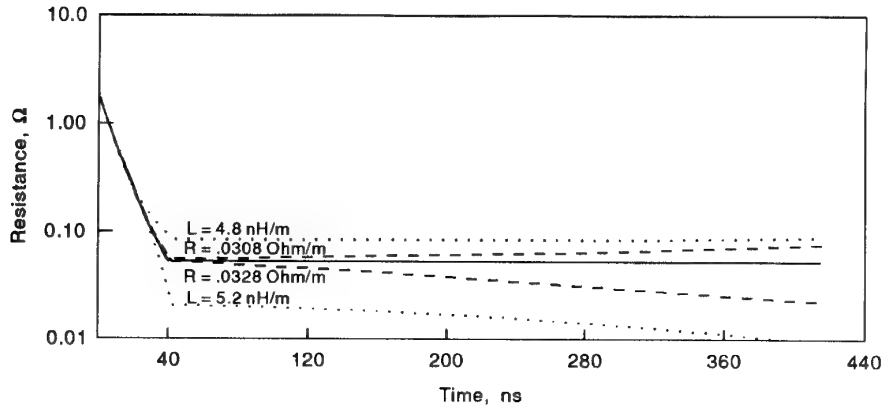

Figure 5: *Effect of variation of transmission line parameters on the modelled switch resistance calculations. Solid line represents the control curve with L = 5.0 nH/m and R = 0.0318 Ω/m. The fine, dashed line represents R = 0.0318 Ω/m and L varying by ± 0.2 H/m. The L = 4.8 nH/m line is shown above the reference and L = 5.2 nH/m below. The coarse dashed line represents L = 5.0 nH/m and R varying by ± 0.0010 Ω/m. The R = 0.0308 Ω/m line is shown above the reference and R = 0.0328 Ω/m below.*

"bending" effect on the resistance curve $r(t)$. This causes some apparent changes in the waveform offset, though the effect is minor compared to the changes in the decay rate compensation, as is evident from the example in Fig. 5. Thus adjustments in L are used mainly to control the offset of $r(t)$ and adjustments in R to control the decay rate of $i(0,t)$. Because of nominal interdependence between the R and L adjustments, the final match between the $r(t)$ waveform calculated according to Eq. (23), and the control $r(t)$ waveform calculated according to Eq. (1), is accomplished after a number of iterations.

Clearly, in the absence of accurate transmission line parameter values, the transmission-line based technique relies on conventional

voltage measurements for its calibration though this is performed under rather special conditions. However, once calibrated, this technique can be extended well beyond the capabilities of conventional methods.

To determine L, C and R in the experimental set-up, shown in Fig. 2, we used an atmospheric gap breakdown (AGB) switch. It consisted of one strip line conductor folding over the other, and was switched by reducing the atmospheric gap between the conductors until spontaneous breakdown occurred. Because of the strip line geometry, the switch self-inductance was kept low. Also, the switching process was smooth and slow enough to permit reasonably accurate voltage measurements across the switch. One example of the AGB current, voltage and resistance waveform is given in Figs. 6(a), 6(b) and 6(c), respectively. Fig. 6(c) shows the switch resistance waveform according to Eq. (1) (fine dashed line) and a superposed switch resistance waveform obtained via Eq. (23) (solid line), using seven integration terms. The transmission line parameters L and R were adjusted to obtain the best possible match between the two waveforms. A slight mismatch in the "knee" of the curve is evident in the 1.0 to 0.1 Ω transition and was found to be caused by the inductive pick-up of the voltage probe. An $\{M\, di(0,t)/dt\}$ correction to the voltage trace leads to a better match if the mutual inductance factor $M \cong 1.5$ nH between the probe and switch circuit is used.

In this calibration, the initial line voltage was $V_0 = 990$ V, and the signal propagation velocity was calculated from the double transit time of the switching wave front yielding a value of $c = (1.55 \pm 0.05) \times 10^8$ m/s. Matching of resistance waveforms according to Eqs. (1) and (23) required adjustments in L and R, yielding $L = 5.0 \pm 0.1$ nH and $R = (2.65 \pm 0.05) \times 10^2\ \Omega/\text{m}$. We then calculated $C = (L\, c^2)^{-1} = 8.3$ nF/m and $Z_0 = c\ L = 0.775\ \Omega$. Calibrations in earlier experiments have shown slightly different values of L and R. In the experiments performed soon after the construction of the 33 m long strip line, the value of $L = 5.3$ nH was determined, which settled down to 5.0 nH after approximately six months. This suggests that during this period, the gap between the strip line conductors has shrunk by approximately 5%. The exact cause of this has not been determined, but we suspect that age-induced shrinkage of the adhesive between the copper strips and the kapton (polyimide) insulator may account for the change. The value of R, on the other hand, changed randomly between experimental runs and is likely to have been caused by temperature fluctuations. The temperature coefficient of resistivity for standard annealed copper [19] is approximately 0.004 $(°C)^{-1}$ at 20°C, resulting in a 4% change in the value of R for temperature changes of 10°C. In absolute terms this represents a change in R of approximately $1 \times 10^{-3}\ \Omega/\text{m}$ per 10°C. Thus, it is advisable to calibrate the transmission line parameters employed in Eq. (23) prior to the start of each experimental run, particularly R.

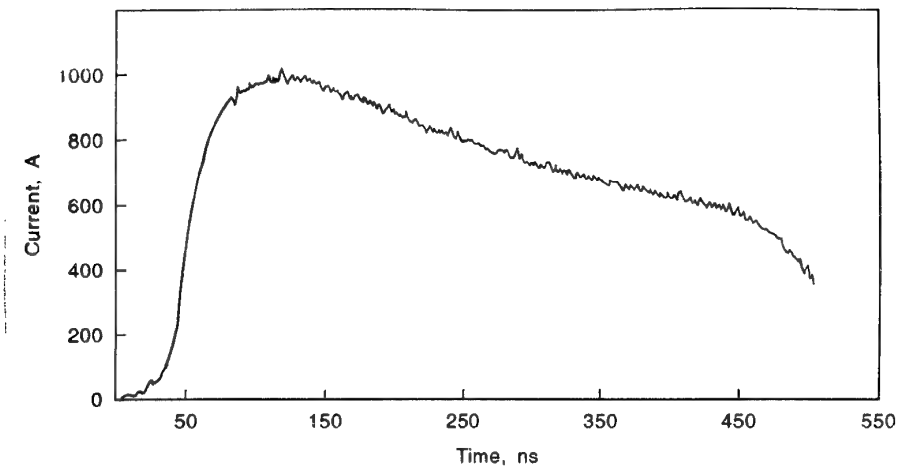

(a)

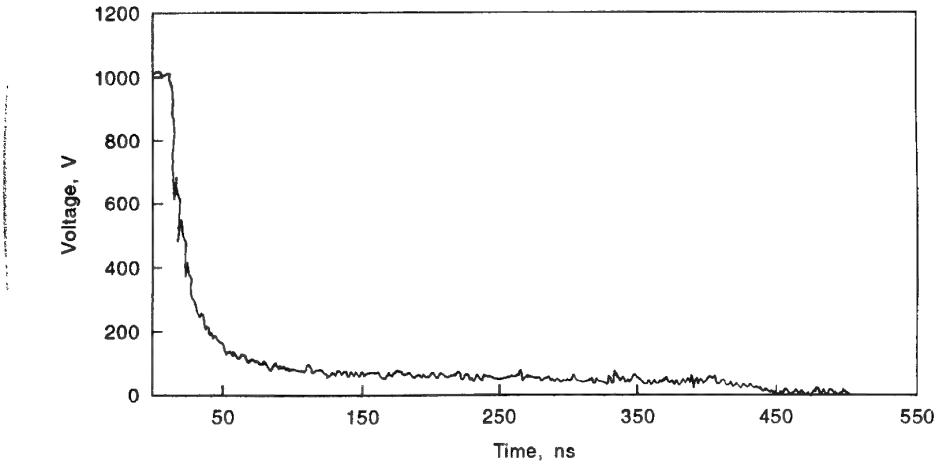

(b)

Figure 6: *(a) shows the current, (b) the voltage, and (c) the resistance waveform of an AGB switch, connected to the parallel strip line, initially charged to 990 V. The fine dashed line in (c) represents r(t) according to Ohm's law and the solid line represents r(t) calculated from transmission line relations. The deviation beyond the 400 ns interval is due to the arrival of the reflected primary wave.*

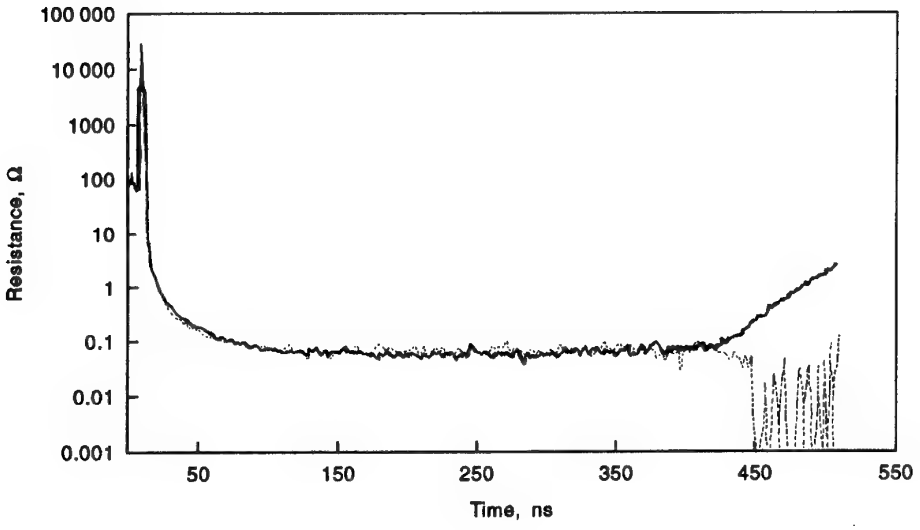

(c)

Figure 6: *(a) shows the current, (b) the voltage, and (c) the resistance waveform of an AGB switch, connected to the parallel strip line, initially charged to 990 V. The fine dashed line in (c) represents r(t) according to Ohm's law and the solid line represents r(t) calculated from transmission line relations. The deviation beyond the 400 ns interval is due to the arrival of the reflected primary wave.*

4.3 Switch Resistance Measurements

After calibration of the transmission line parameters, other switches were investigated. The first presented here is a triggered vacuum gap switch TVG-4.[4] Compared with the AGB switch, it also performs relatively smoothly and therefore enabled reasonably accurate direct voltage measurements. The current, voltage and resistance curves, presented in Figs. 7(a) - 7(d), were obtained from an experiment performed at $V_0 = 1007$ V, soon after the construction of the strip line. Fig. 7(c) shows the switch resistance waveform obtained according to Eq. (1) as a fine dashed curve, whereas the waveform obtained according to Eq. (23) is shown as the solid curve. The main difference between the two curves is due to the inductive pick-up of the voltage probe and can be corrected for if a mutual inductance factor of approximately 1.5 nH is used. The switch resistance calculated with the corrected voltage

[4]The triggered vacuum gap switch TVG-4 was part of an experimental batch produced by English Electric Valve Co. Ltd., Essex, UK.

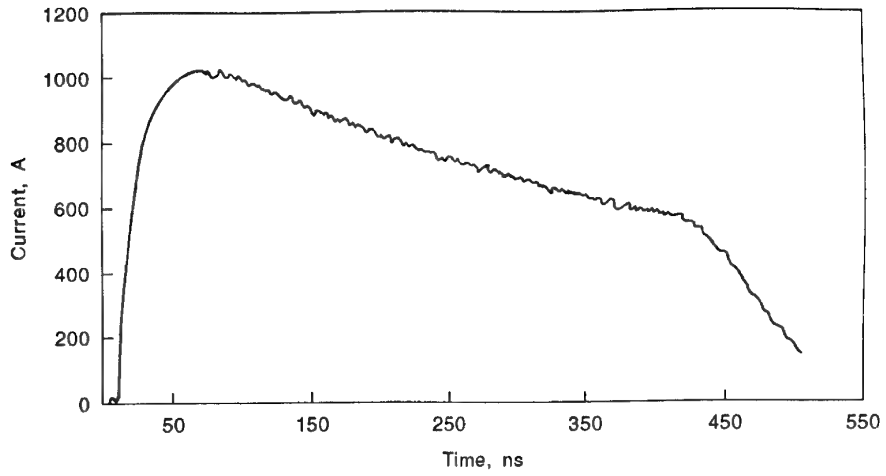

(a)

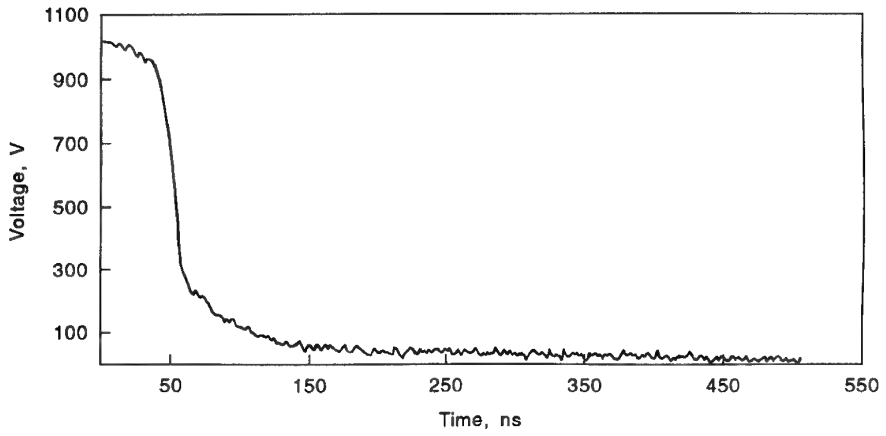

(b)

Fig. 7 The TVG-4 switch operated at line voltage of 1007 V. The switch current waveform is shown in (a), the voltage waveform in (b) and the resistance waveform in (c) and (d). The fine dashed line in (c) represents the resistance calculated from the switch current and voltage according to Ohm's law, whereas the solid line shows the resistance calculated from the transmission line relations. Part (d) is identical to (c) except a correction to the finely dashed curve, compensating for the inductive pick-up component in the voltage waveform.

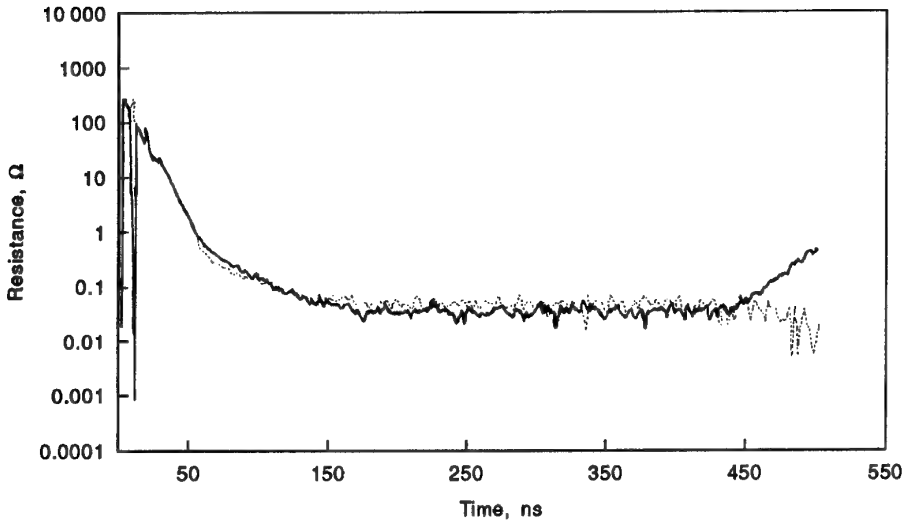

(c)

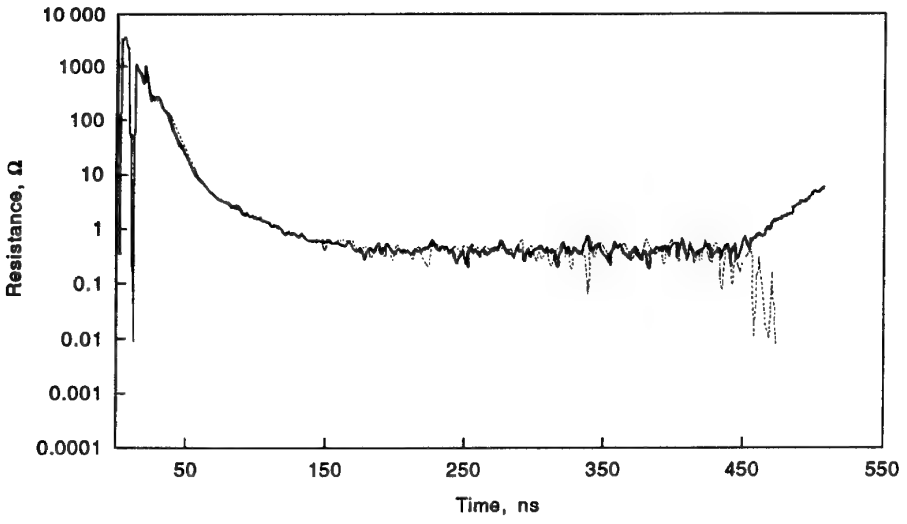

(d)

Fig. 7 The TVG-4 switch operated at line voltage of 1007 V. The switch current waveform is shown in (a), the voltage waveform in (b) and the resistance waveform in (c) and (d). The fine dashed line in (c) represents the resistance calculated from the switch current and voltage according to Ohm's law, whereas the solid line shows the resistance calculated from the transmission line relations. Part (d) is identical to (c) except a correction to the finely dashed curve, compensating for the inductive pick-up component in the voltage waveform.

according to Eq. (1) is represented by the fine dashed curve in Fig. 7(d) and shows better agreement with the resistance curve obtained through Eq. (23) (solid line). The transmission line parameters used in the calculations were $L = 5.3$ nH/m, $R = 2.65\times10^{-2}$ Ω/m and $c = 1.55\times10^{8}$ m/s. Consequently, $Z_0 = 0.82$ Ω and $C = 7.8$ nF/m.

The second switch tested, referred to here as the explosive actuated (EA) switch [20,21], has probably the most intricate behaviour compared with the two previous ones. In fact, it is the complex behaviour of this switch that motivated the development of the transmission-line based technique so that a time-dependent resistance waveform could be obtained with a signal bandwidth reaching 200 - 400 MHz. The switch is based on a flying plate, accelerated by an explosive charge, impacting and penetrating a charged strip line, resulting in a mechanical failure and subsequent electrical breakdown of the gap between the conducting strips. In our experiments, the flying plate was made from a round copper disc, approximately 3 mm in diameter and 0.4 mm thick, and the strip line, akin to the one portrayed in Fig. B1, was made from a copper-adhesive-kapton-adhesive-copper laminate approximately 0.15 mm thick. Impact velocities were estimated to range between 2×10^{3} and 3×10^{3} m/s.

Four examples of the EA switch resistance measurement are given. The first two refer to an experiment performed with the 33 m long parallel strip line at $V_0 = 942$ V and $V_0 = 2000$ V. The resultant current and resistance waveforms are given in Figs. 8(a) - 8(c) and Figs. 9(a) - 9(c), respectively. In comparison with the current waveforms in Figs. 6(a) and 7(a), the EA switch current waveforms in Figs. 8(a) and 9(a) display significant irregular fluctuations in the high as well as the low frequency region. The strip line parameters used were $L = 5.0$ nH/m, $c = 1.55\times10^{8}$ m/s and $R = 0.0265$ Ω/m.

The third and fourth examples refer to experiments employing a 100 m long co-axial cable, with a nominal characteristic impedance $Z_0 \cong 50$ Ω. For the initial line voltages $V_0 = 397$ V and $V_0 = 2000$ V, the switch current levels were approximately 60 times lower than for the 0.8 Ω strip line. However, the same laminate-based EA switch configuration was used and connected to the 50 Ω transmission line, with the current monitored by a Tektronix CT-2 current transformer (the bandwidth of the CT-2 probe is specified as 30 kHz to 1 GHz).

The current, voltage and resistance waveforms for $V_0 = 397$ V experiment are shown in Figs. 10(a) to 10 (c), and the current and resistance waveforms for $V_0 = 2000$ V in Figs. 11(a) and 11(b). The irregularities in the switching waveforms are believed to be caused by the copper disk's shearing of the strip-line laminate, resulting in a rather erratic behaviour of the gap breakdown. Significant differences between the strip line and co-axial line based experiments are evident, however. Firstly, the current and resistance waveforms in the co-axial line experiments are considerably less noisy than the stripline ones. This suggests the possibility that the normally negligible inductive component of the CVR is significant enough to accentuate the high frequency components of the current waveform.

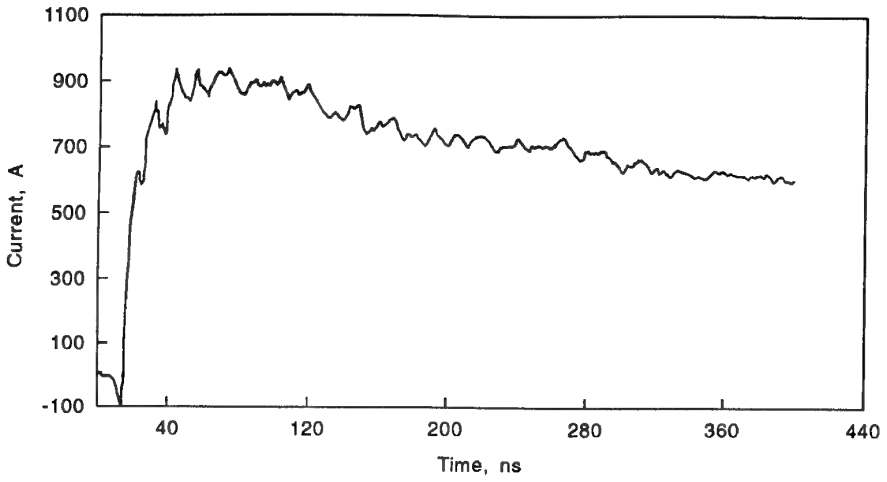

(a)

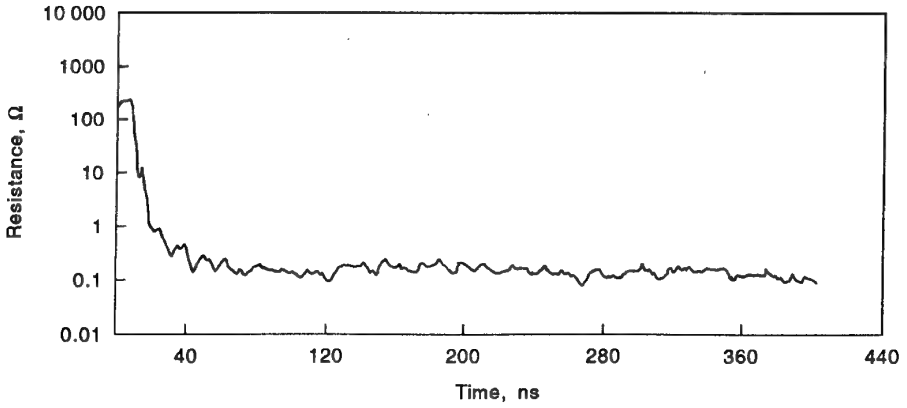

(b)

Figure 8: *An EA switch experiment using the parallel strip line, charged initially to 942 V. The current waveform is shown in (a), and the resistance, calculated from transmission line relations, in (b) and (c). The resistance in (b) is displayed on a logarithmic scale over a 400 ns time interval, whereas in (c) a more detailed view is given using a linear scale over a 200 ns time interval.*

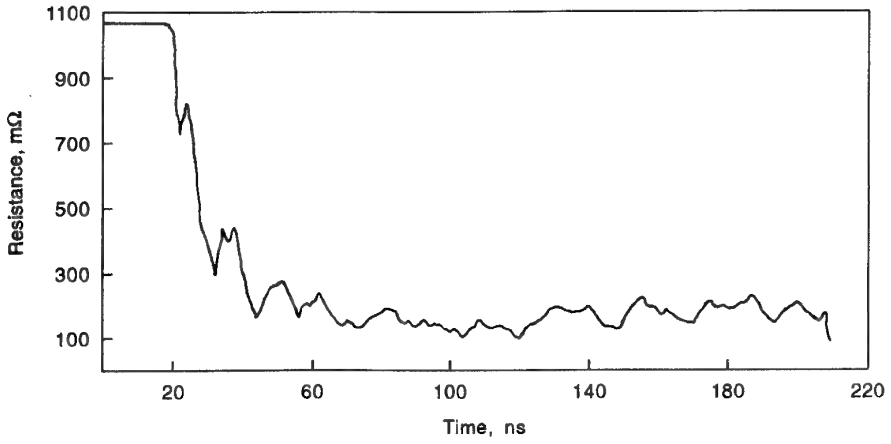

(c)

Figure 8: *An EA switch experiment using the parallel strip line, charged initially to 942 V. The current waveform is shown in (a), and the resistance, calculated from transmission line relations, in (b) and (c). The resistance in (b) is displayed on a logarithmic scale over a 400 ns time interval, whereas in (c) a more detailed view is given using a linear scale over a 200 ns time interval.*

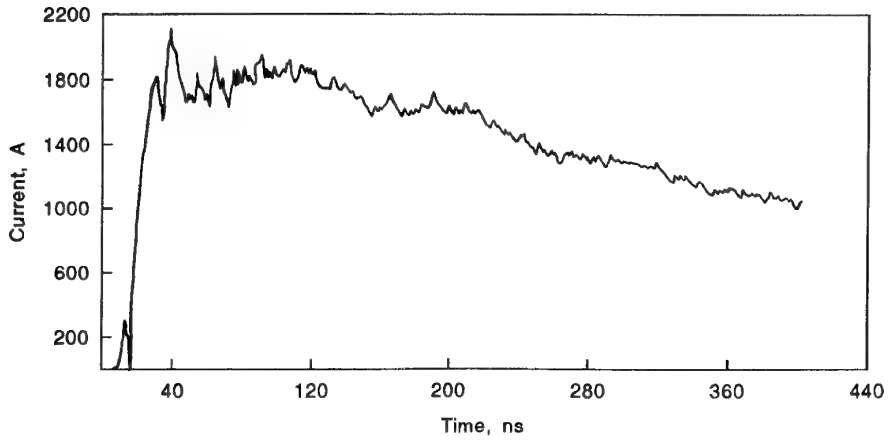

(a)

Figure 9: *EA switch experiment as in Fig. 8, but with initial line voltage of 2000 V. The switch resistance waveforms in (b) and (c), represented by solid curves, have been smoothed (fine dashed curves) to portray the more slowly varying characteristic of the switch resistance.*

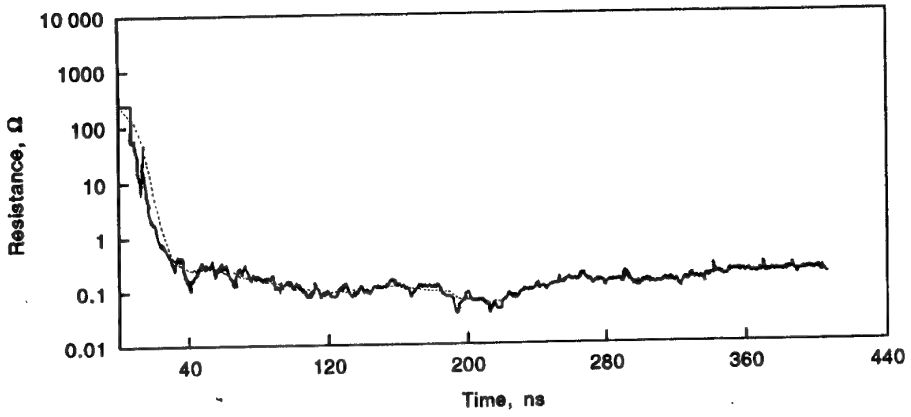

(b)

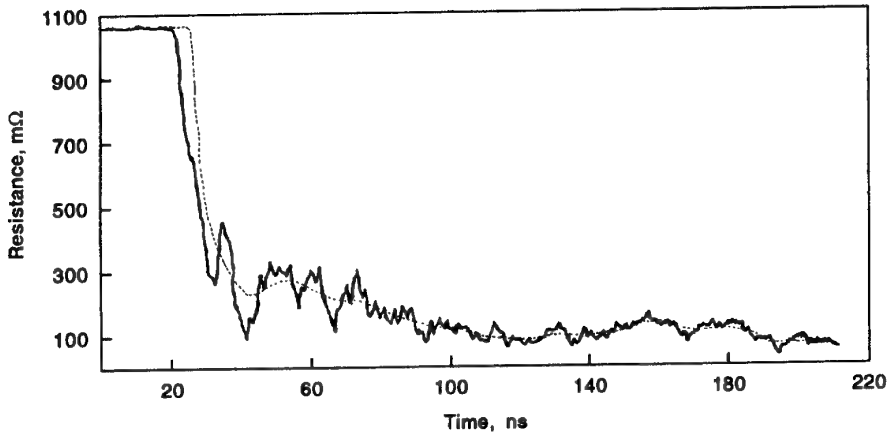

(c)

Figure 9: *EA switch experiment as in Fig. 8, but with initial line voltage of 2000 V. The switch resistance waveforms in (b) and (c), represented by solid curves, have been smoothed (fine dashed curves) to portray the more slowly varying characteristic of the switch resistance.*

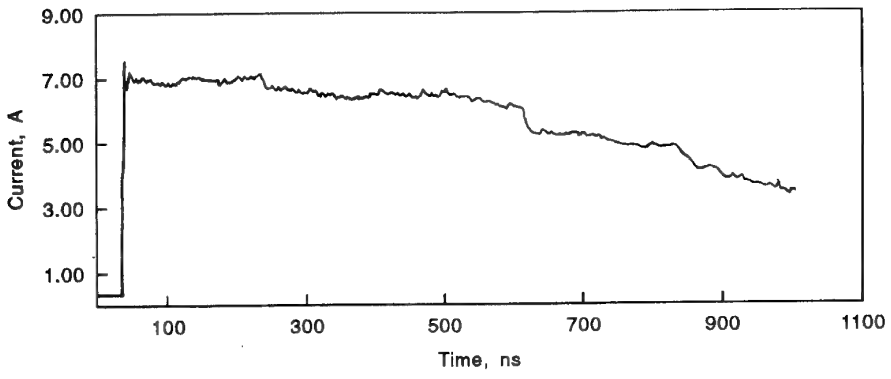

(a)

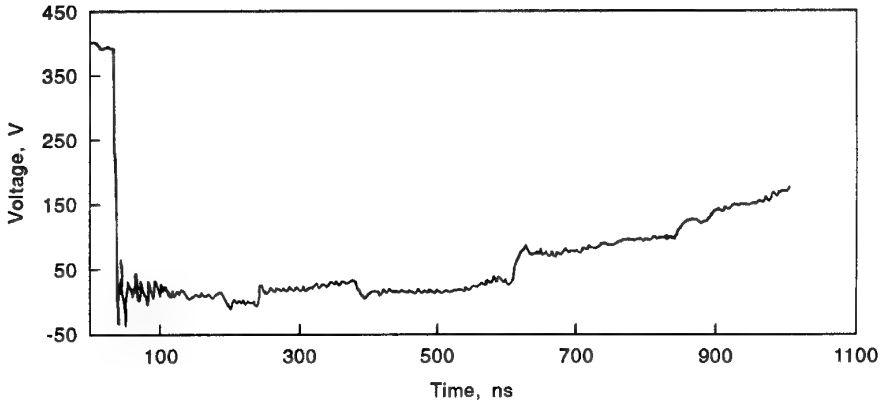

(b)

Figure 10: *An EA switch experiment using the 50 Ω co-axial transmission line, charged initially to 397 V. The current waveform is shown in (a), the voltage waveform in (b) and the resistance in (c). The fine dashed line in (c) represents the resistance calculated from the switch current and voltage according to Ohm's law and shows significant high frequency noise when compared with the solid line which represents the resistance calculated from transmission line relations.*

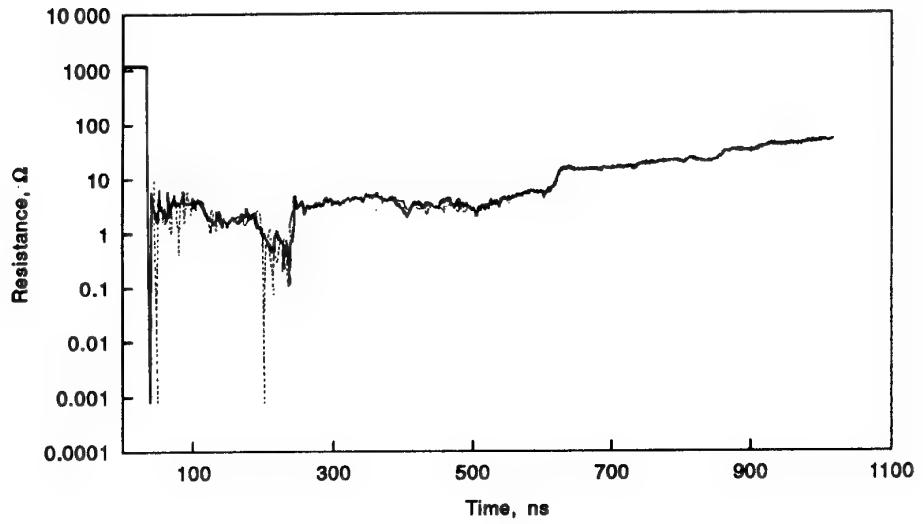

(c)

Figure 10: *An EA switch experiment using the 50 Ω co-axial transmission line, charged initially to 397 V. The current waveform is shown in (a), the voltage waveform in (b) and the resistance in (c). The fine dashed line in (c) represents the resistance calculated from the switch current and voltage according to Ohm's law and shows significant high frequency noise when compared with the solid line which represents the resistance calculated from transmission line relations.*

Secondly, the minimum levels of the switch resistance achieved in the co-axial line experiments are about an order of magnitude higher that the stripline ones. This can be loosely ascribed to the non-linear behaviour of the EA switch, since the transmission line impedance limits the maximum possible current level flowing through the switch according to $i(0,t)_{max} \leq V_0 / Z_0$. Experiments with the 0.8 Ω stripline at charge voltages of $V_0 = 40$ V have produced similar switch currents as those for the 50 co-axial line for $V_0 = 2000$ V, as well as similar switch-closure resistance values. The higher closure-resistance levels observed at low charge voltages (< 50 V) is consistent with the observed trends reported in [21].

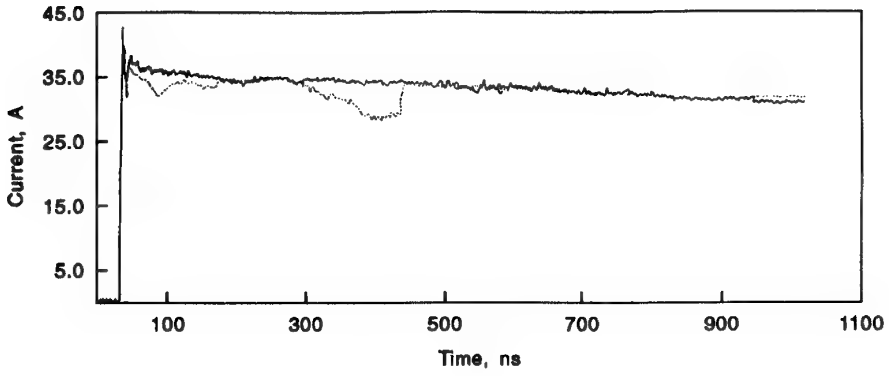

(a)

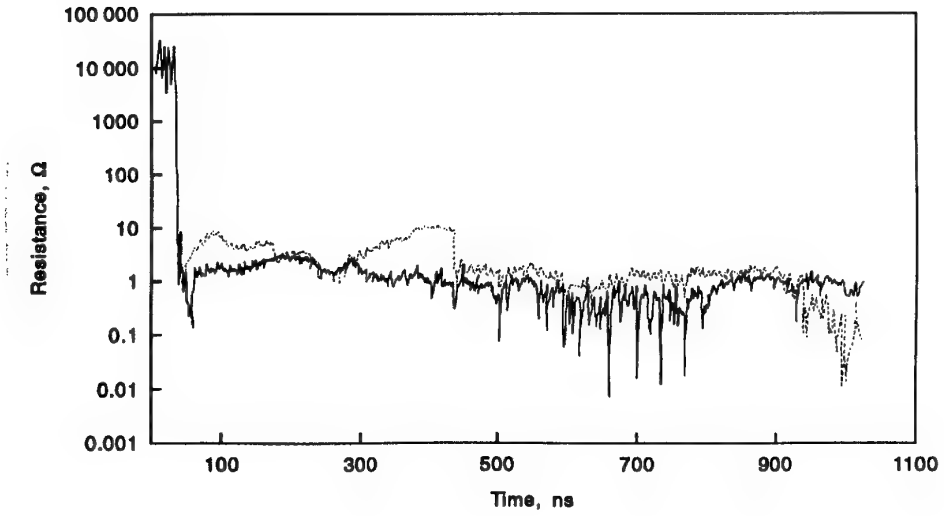

(b)

Figure 11: *Two EA switch experiments using the 50 Ω co-axial transmission line, charged initially to 2000 V. The current waveforms are shown in (a) using a solid and fine dashed line. The respective resistance waveforms, calculated from transmission line relations, are shown in (b).*

Since the process of flyer penetration through the switch stripline is expected to be quite complex, it is difficult to speculate how the various physical processes affect the switch resistance characteristics. Nonetheless, many switch resistance traces [21] show a noticeable change in the current/resistance level, approximately 120 to 200 ns after current onset (this is also evident in the current traces of Figs. 8(a), 9(a) and 10(a)). Such a change could be associated with the passage of explosive by-products behind the flyer after the flyer ceased making direct contact with the copper layers of the switch stripline during the penetration of the 7.5×10^{-5} m thick insulating layer in between. With flyer thickness of about 4×10^{-4} m and velocity of approximately 2×10^{3} to 2.5×10^{3} m/s, the direct contact of the flyer with the stripline is estimated to lie roughly in the rage of 100 to 200 ns.

For some slapper detonator designs the state of the switch resistance is no longer critical beyond about 100 ns and any subsequent changes in the switch conduction would be irrelevant. It may be added that if the switch conduction consists of distinct processes dependent on the stripline penetration by the flyer, like the one suggested above, then factors such as flyer planarity/attitude, speed or material type could play a significant role in the time-dependent switch resistance characteristics. Three experiments performed with 0.5 mm polycarbonate flyers [21] resulted in waveforms similar to those with copper flyers, but the waveforms were less noisy and displayed longer switch-closure time.

The 50 Ω co-axial line based experiments provide a good example of the effect of higher value of Z_0 on the switch resistance measurement technique. We found that within several nanoseconds, the switch resistance $r(t)$ dropped to a very small fraction of Z_0, so that $r(t) / Z_0 \approx 0$ and the switch resistance could be considered quasi-constant. In such case, Eq. (28) and the decay rate of the current waveform is governed by a simple exponential term $e^{-t\delta/2}$ for such t, where $r(t) << Z_0$. Practical attempts at correcting the decay term in the resistance waveform with this simple exponential term were quite successful, provided that the switch-closure time was fast and the onset of switch current could also be assumed to be the time origin for the exponential correction factor.

The 50 Ω co-axial transmission line parameters obtained from calibrations based on the $V_0 = 397$ V example data were: $L = 275$ nH/m, $c = 2.0\times10^{8}$ m/s and $R = 0.10$ Ω/m, with implied $C = 91$ pF/m and $Z_0 = 55$ Ω. The fact that the cable impedance Z_0 is rated at 50 Ω, suggests that some scaling errors may have occurred during measurement of current and/or voltage. For instance, it can be shown, that a 10% increase in the scaling factor of the switch current would result in $L = 250$ nH/m and $C = 100$ pF/m which yields the rated value of $Z_0 = 50$ Ω. The scaling effect is discussed further in Section 5.

5. Discussion

The theoretical development, and the modelled and practical examples have illustrated the viability of the transmission-line based method of resistance measurement for single-shot, high speed closing switches. However, the advantages gained, such as increased measurement bandwidth and reduction in the inductive pick-up noise are partly offset by other inaccuracies. Below, we discuss the effect of measurement errors on the accuracy of the calculated switch-resistance waveform and the effect of choice of the transmission line's value of characteristic impedance.

5.1 Errors in Switch Resistance Waveform Determinations

5.1.1 Significance of Errors in Calibration Experiments

The calibration of the transmission line parameters is paramount to the success of this measurement technique, and as we have shown, this can be accomplished by matching the resistance waveform calculated according to Eq. (23) with a conventionally determined waveform calculated according to Ohm's law in Eq. (1). Hence, the calibration is affected by the uncertainty and errors in the voltage and current measurements, and any subsequent transmission line measurements based on these calibrations will propagate these errors. However, the calibration tests can be performed for signals under optimal conditions which yield the best possible voltage and current measurement accuracy. The level of accuracy obtained from these tests is then extended into measurements which are well beyond the scope of the more conventional techniques. Because certain transmission line parameters, eg., the distributed resistance R, can fluctuate over a period of time, it is recommended that calibration tests be performed at the start of each experimental run.

5.1.2 Effect of Scaling Errors and Value of Z_0 in Calibration measurements

If a scaling error occurs either in the current or voltage measurement, or both, then it is linearly propagated as a fractional error into the switch resistance waveform, calculated according to Eq. (1). In the transmission-line based method, however, this error may be considerably amplified because of the form of Eq. (23). Since $i(0,t) < 0$ for $V_0 > 0$, the right-hand side of Eq. (23) consists of two difference terms, containing Z_0 and V_0, respectively. It is evident from Eq.(23) that a scaling error in $i(0,t)$ or V_0 affects the absolute error in the V_0 term and therefore the error in $r(t)$. If $r(t) << Z_0$, the magnitude of the error in $r(t)$ may become many times larger than the magnitude of $r(t)$ itself. However, provided that the scaling error is systematic, it is

possible to absorb some of its effect through the adjustment of transmission line parameters in calibration tests.

Scaling errors of 10% to 20% can be readily accommodated in the adjustment of transmission line parameters without significant loss of accuracy of the technique relative to the reference waveforms. Inspection of Eq.(23) shows that scaling errors in $i(0,t)$ affect the V_0 term. This error can be compensated by altering the value of Z_0 though this will in turn affect the value of δ. Using the numerically simulated example, excellent adjustments were obtained for 10% variations in either the current $i(0,t)$ or the initial line voltage V_0. Scaling inaccuracies may well explain the apparently higher than expected value of Z_0 encountered in the 50 Ω co-axial line experiments or the lower than expected value of R in the parallel strip line set-up.

In the calculation of switch resistance according to Eq. (23) the transformation from a fractional error (as in Eq.(1)) to an absolute type cannot be eliminated, but it can be reduced to acceptable levels by using a transmission line for which $r(t) \sim Z_0$.

5.2 *Practical considerations*

In practical applications of the transmission-line based method, the simple form of Eq. (24) is preferred to that of Eqs. (23) or (28). Eq. (24) holds well for transmission lines where the waveform is not appreciably affected by the dissipative losses within the time interval of interest. Inspection of Eq. (27) shows that Eq. (24) provides a good approximation if R/L or t is small, or $(r_0 + Z_0)$ is large. If, however, the use of Eq. (23) cannot be avoided, other problems may arise such as numerical overflow in the evaluation of the successive integration terms. This is prevented by adopting a nested integration approach according to

$$r(t) = -\frac{Z_0}{i(0,t)}\left[i(0,t) + \left(\frac{\delta}{2}\right)\left\{ \int_{t=0}^{t} i(0,t)dt - \left(\frac{\delta^2}{8}\right)\left\{ \int_{t=0}^{t} i(0,t)dt + \ldots \right.\right.\right.$$

$$\left.\left.\left. \ldots + \frac{\delta^k (1/2)!}{(1/2-k)!k!} \int_{t=0}^{t} i(0,t)dt \ldots \right\} dt \right\} dt \right] - \frac{V_0}{i(0,t)}, \qquad (29)$$

commencing calculations from the innermost bracket. Clearly, a practical limit exists on the number of integration terms that may be used in the switch resistance calculation. Hence, this limits the length of the time interval within which the switch resistance can be accurately evaluated, though other competing restrictions exist by virtue of assumptions made in the derivation of Eq.(23).

5.3 *Nonlinearity of Switch Behaviour*

In a slapper detonator application, the nature of the switch may be such that its resistance is not exactly the same as the one obtained during the transmission-line discharge test. The difference may be due to the LCR character of the slapper detonator circuit, eg. [4], coupled with possible non-linear aspects of the switch behaviour. Hence, it is important to test the switch over a range of voltages and currents in order to define the switch characteristics as close to the actual operating state as possible. In the case of the explosively actuated switch, the closure time and resistance were, on average, reasonably constant within the range of 100 V to 2000 V [21]. At charge voltages below 50 V, the switch resistance tended to increase markedly with decreasing voltage and the switch resistance waveforms were prone to be much more irregular.

5.4 *Effect of Switch Inductance*

In our treatment so far, we were able to neglect switch inductance because of the low inductance switches used in our tests. For some other types of switches, however, such convenient assumption may not be always possible and a term, $-\{d[L_s(t)i(0,t)]/dt\}/i(0,t)$, would have to be added to the right hand side of Eq. (23) with $L_S(t)$ representing the time-dependent switch inductance. In practice, $L_S(t)$ is generally difficult to determine and would complicate the switch resistance determination accordingly.

A realistic, but simple case of constant switch inductance illustrates the type of effect that switch inductance may have on the resistance waveform. In such an instance the inductive term $-\{d[L_s(t)i(0,t)]/dt\}/i(0,t)$ simplifies to $-L_s\{di(0,t)/dt\}/i(0,t)$. This has the general effect of increasing the apparent value of switch resistance $r(t)$, while the switch current is increasing, and the converse holds true in those instances where the current decreases.

5.5 *Frequency Dependence of Transmission Line Parameters*

In the transmission-line-based method of switch-resistance measurement, we have assumed constant and uniform transmission line parameters L, C, R and G. In Section 2.2.2, we have given reasons for assuming $G = 0$. Below, we outline the frequency dependent behaviour of the other parameters and discuss the significance of this in relation to the switch resistance measurements. While much of the underlying theory may be found in a number of textbooks on transmission line theory, we draw mainly on the work of Chipman [14] and Grivet [15].

5.5.1 *Frequency Dependence of C and L.*

As stated in both Ref. 14 and 15, there is no electric field within the transmission-line conductors and the electric charges reside on the surface of the conductors. This electric field distribution is independent of the signal frequency and hence the distributed capacitance of a uniform transmission line remains constant with frequency.

However, the line inductance is subjected to variation with frequency. This is due to the existence of magnetic field within the transmission-line conductors [14,15]. In general, the line inductance may be divided into two components, external and internal. The current flow within the transmission line conductors gives rise to external and internal magnetic fields which are the basis of the external and internal inductance components, respectively.

As explained in Refs. 14 and 15, the current and magnetic field distribution within the current carrying conductors changes with frequency. As the signal frequency increases, the current distribution becomes increasingly concentrated close to the surface of each current-carrying conductor. This is commonly referred to as the "skin effect". The skin effect affects the internal magnetic field distribution and hence the internal inductance component, whereas the external distribution remains unaltered.

In the transmission lines used in our experiments, the external inductance component dominates the internal one and therefore, no significant frequency-dependent behaviour of the lines' distributed inductance is expected. This is mainly due to the small thickness of the transmission-line conductors relative to the gap between them [14,15]]. In order to ensure negligible effect of line inductance variation with frequency, the conductor gap-to-thickness ratio should be kept suitably large in the design of transmission lines for switch resistance measurement .

5.5.2 *Frequency Dependence of R*

The frequency dependence of R is due to the skin effect (see for example Refs. 14 and 15). Out of the four transmission line parameters, R is the one most affected by frequency changes.

As frequency increases, the current is increasingly concentrated near the surface of the conductors. This is approximately expressed by the skin depth term δ_s, which gives the thickness of the conductor that would carry an equivalent dc current. For an infinite planar conductor, the skin depth is defined as $\delta_s = \sqrt{2\rho_0/\omega\mu}$, where ρ_0 is the dc resistivity of the conductor material [14]. The skin depth definition will vary somewhat with the conductor geometry, but the one given here serves as a reasonable approximation for both the stripline as well as the coaxial line.

While the conductor thickness is of the order of one skin depth or less, the skin effect will not affect the line's distributed resistance R.

However, once the conductor thickness becomes large compared with δ_s, then R will increase with frequency as $R \propto \sqrt{\omega}$.

The influence of the skin effect on the variation of R can be minimised by the design of the transmission line. First, the thickness of the conductors should be kept to a minimum and second, the line inductance should be maximised. The reason for this arises from the combined effect of the line inductance L and the line resistance R on the transmission line impedance Z, defined from Eqs. (14) and (15) as $Z = V(x,s)/I(x,s)$, namely

$$Z = \sqrt{\frac{Ls + R}{G + Cs}} \tag{30}$$

If $Ls >> R$, then the effect of R on the transmission line current will be negligible. When skin effect becomes important then Eq.(30) can be rewritten as

$$Z \cong \sqrt{\frac{Ls + K\sqrt{s}}{G + Cs}}\ , \tag{31}$$

where $K\sqrt{s}$ is related to the skin depth formula, with s being the complex frequency.

From Eq.(31) it is evident that at sufficiently high frequencies, the Ls factor will dominate and therefore, the skin effect will not affect the switch resistance calculations. However, there exists an intermediate frequency range where the $K\sqrt{s}$ factor has the maximum effect. For example, the conductor thickness for our stripline is equal to one skin depth at signal frequency of 3.5 MHz. At this frequency $R \cong 0.0318\,\Omega/\mathrm{m}$ and $L\omega \cong 0.114\,\Omega/\mathrm{m}$. A simplified estimate shows that the error in R due to the skin effect will result in switch resistance errors which are not expected to exceed the 10 - 15% level for frequencies between 7 - 200 MHz. This error estimate is shown in Fig. 12 as a function of frequency and is obtained from the relation

$$\Delta\eta = e^{-\frac{R}{2L}\Delta t} - e^{-\frac{R'}{2L}\Delta t}\ , \tag{32}$$

where $\Delta\eta$ is the fractional error and is calculated from a simple decay estimate based on Eq. (28). In fact, Eq. (32) represents the fractional error in $r(t) + Z_0$ for a quasi constant switch resistance $r(t)$ over a time interval $\Delta t \approx 2\pi/\omega$. The skin-effect-dependent resistivity is defined as $R' \cong R\sqrt{\omega/\omega_0}$ for $\omega \geq \omega_0$, where the conductor thickness of the transmission line is equal to one skin depth at frequency ω_0.

The above estimates illustrate that the magnitude of the error due to the skin effect may not be negligible, though the actual levels are difficult to estimate and are also dependent on other factors such as the characteristic impedance of the transmission line as well as the

magnitude of the switch resistance itself. The larger the ratio of $r(t)/Z_0$, the smaller is the effect of frequency dependent variation of R.

In our experiments, we have not observed any gross deviation which could be accounted for through skin effect. The higher frequency changes in the measured switch resistance occurred during the initial closure of the switches, and during these changes the value of $r(t)/Z_0$ was relatively high. Also, the calibration of the transmission line parameters would have partly disguised the presence of any errors due to skin effect.

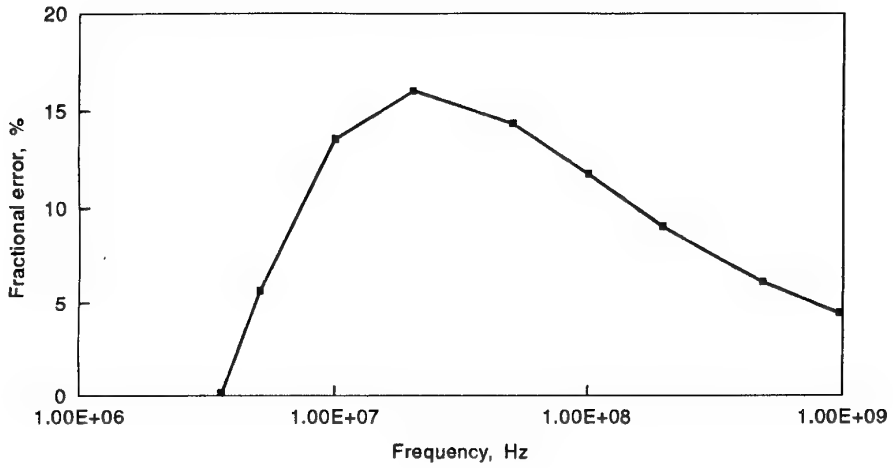

Figure 12: *Approximate error estimate in the switch resistance calculation due to skin effect in the experimental parallel stripline.*

6. Conclusion

The transmission-line based method of time-dependent resistance measurement of single-shot closing switches shows considerable promise for applications demanding high bandwidth under high current, high voltage conditions. The method requires an initial calibration of the transmission line's parameters, such as the distributed inductance, capacitance and resistance. However, after calibration, only the switch current and the initial charge voltage of the line need to be measured. Also, we have provided a theoretical

formulation of the switch resistance calculation which allows for the lossy behaviour of practical transmission lines.

It was found that good accuracy is achieved when the switch resistance magnitude is of similar order as the transmission line's characteristic impedance, or higher. To the extent that this condition cannot be met, it is necessary to increase the accuracy of all measured quantities, including the calibrations of the transmission line parameters. Also, it is important to consider the frequency dependent behaviour of the transmission line's resistivity due to the skin effect, though this can be minimised through careful transmission line design.

With the aid of our transmission line model, we found that the calibration of transmission-line parameters is able to accommodate sizeable scaling inaccuracies that may exist in the reference voltage and current waveforms. These errors may therefore propagate into any subsequent transmission-line based resistance measurements.

Since the switch resistance characteristic is determined under special circumstances, i.e., the transmission line discharge technique, one needs to exercise caution when using the results in specific applications because of possible non-linearities in the switch behaviour.

7. Acknowledgments

The support and advice of Mr. G. K. Manzie is gratefully acknowledged and particular thanks are due to Mr. A. R. Harrison, who assisted with the construction of the apparatus, running of the experiments and some of the initial theoretical developments while working under the Vacation Scholar program. Also, the author wishes to express his gratitude to Dr. D. D. Richardson and Messrs. J. D. Oliver, J. A. Waschl and B.E. Jones for advice and technical assistance in the work. A number of pertinent comments from Dr. I. Sach are also gratefully acknowledged.

8. References

1. Richardson, D.D. (1987).
Studies on Slapper Detonators (U) (MRL Report MRL-R-1083) (Confidential).
Maribyrnong, Vic.: Materials Research Laboratory.

2. Waschl, J.A. (1988).
Performance Measurement of Slapper Detonator Systems (HDL Report HDL-PP-TAO-88-1).
U.S. Army Laboratory Command, Adelphi, MD.: Harry Diamond Laboratories.

3. Hatt, D.J. and Waschl J.A. (1991).
Performance Evaluation of an EBF Generated thin Flyer Plate (U) (MRL Report MRL-TR-91-28) (Limited Release).
Maribyrnong, Vic.: Materials Research Laboratory.

4. Ryan P.F., Jones B.E., and Richardson D.D. (1989).
A medium scale flying plate generator (MLR Report, MRL-RR-2-89).
Maribyrnong, Vic.: Materials Research Laboratory.

5. Podlesak M., Richardson D.D. and Olsson C. (1993)
An Exploding Foil Flying Plate Generator for Shock Wave Studies - Calibrations (MLR Report, MRL-RR-1-92).
Maribyrnong, Vic.: Materials Research Laboratory.

6. Chau, H.H., Dittbenner G., Hofer W.W., Honodel C.A., Steinberg D.J., Stroud J.R., and Weingart R.C. (1980).
Electric Gun: a versatile tool for high-pressure shock-wave research.
Review of Scientific Instruments, Vol. 51 (12).

7. Barnes G. and Dannenberg R.E. (1980).
Transient solution for megajoule energy release in a lumped-parameter series RLC circuit. *Journal of Applied Physics*, Vol. 51 (1).

8. Knoepfel H. (1970).
Pulsed High Magnetic Fields, North-Holland, The Netherlands.

9. Podlesak M. (1990).
Rogowski coil calibration on a capacitive discharge rig without the use of a current reference. *Review of Scientific Instruments*, Vol. 61 (2).

10. Tasker D.G. and Lee R.J. (1986)
High Current Electrical Conduction of Pressed Condensed Detonating Explosives", in *Shock Waves in Condensed Matter*, Plenum Publishing Corporation.

11. Hemsing W.F. (1983).
Four Terminal Voltage Probe. *Eighth Firing Systems Conference, Sandia National Laboratories, Albuquerque NM, October 13-13, 1983.*

12. Tucker T.J. (1960).
Square-Wave Generator for the Study of Exploding Wires. *Review of Scientific Instruments*, 31 (2).

13. Goldman S. (1949).
Transformation Calculus and Electrical Transients. Prentice-Hall, New York.

14. Chipman R.A., (1968).
Theory and Problems of Transmission Lines. Schaum outline series, McGraw-Hill, New York.

15. Grivet P. (1970).
The Physics of Transmission Lines at High and Very High Frequencies, translated from French by P. W. Hawkes, Academic Press, London, Vol.1.

16. Thomson W.T. (1957).
Laplace transformation. Longmans, Green and Co., London.

17. Spiegel M.R. (1965).
The Theory and Problems of Laplace Transforms. Schaum Publishing Co., New York.

18. Asystant GPIB (1988).
Asyst Software Technologies, Inc., New York, USA.

19. Skilling H.L. (1951)
Electric transmission lines. 1st ed., McGraw-Hill, New York.

20. Richardson D.D. and Jones D.A. (1986).
A fast, low resistance switch for small slapper detonators. (MRL Report MRL-R-1030).
Maribyrnong, Vic.: Materials Research Laboratory.

21. Podlesak M. (1994)
Electrical Performance of Explosive-Driven Switches for Slapper Detonator Applications. *Propellants, Explosives, Pyrotechnics.* (in press)

Appendix A

Numerical Transmission Line Model

In this work, numerical simulations of a uniform one-dimensional transmission line are based on an approximate representation using a distributed, lumped parameter network, as shown in Fig. A1. The transmission line is subdivided into n segments, where 0, 1, 2, . . , j-1, j, j+1, . . , n, represent the successive nodes in the upper section of the segmented transmission line model. R, L, C and G are the lumped line parameters derived from a transmission line with total resistance R_T, total inductance L_T, total capacitance C_T and total conductance G_T, so that $R = R_T/n$, $L = L_T/n$, $C = C_T/n$ and $G = G_T/n$. The switch resistance $r(t)$ terminates the line at node 0 and a high terminating resistance R_t simulates the open circuit condition at node n.

Eqs. (2) and (3) are rewritten in a discrete form as

$$-\frac{\Delta v(x,t)}{\Delta x} = L\frac{\Delta i(x,t)}{\Delta t} + Ri(x,t) \tag{A.1}$$

$$-\frac{\Delta i(x,t)}{\Delta x} = C\frac{\Delta v(x,t)}{\Delta t} + Gv(x,t) \tag{A.2}$$

Rewriting Eqs. (A.1) and (A.2) in terms of nodal currents and voltages according to Fig. A1, we obtain

$$L\frac{(\Delta i)_j}{\Delta t} = v_{j-1} - v_j - i_{j-1}R \tag{A.3}$$

$$C\frac{(\Delta v)_j}{\Delta t} = i_{j-1} - i_j - v_{j-1}G \tag{A.4}$$

In the model, new values of currents and voltages in each segment are calculated recursively from Eqs. (A.3) and (A.4) according to

$$i_j = i_j + (\Delta i)_j \tag{A.5.1}$$

with

$$(\Delta i)_j = (v_{j-1} - v_j - i_{j-1}R)\Delta t/L \tag{A.5.2}$$

and

$$v_j = v_j + (\Delta v)_j \tag{A.6.1}$$

with

$$(\Delta v)_j = (i_{j-1} - i_j - v_{j-1}G)\Delta t/C \tag{A.6.2}$$

The numerical code written for the transmission line simulation sets firstly the initial values i_j and v_j and then calculates recursively the new values according to Eqs. (A.5.1) to (A.6.2), for nodes 1 to n-1. Different calculations must be performed at the terminations, node 0 and n, which set the boundary conditions. The model calculation at node 0, the switch end, is

$$v_0 = -i_0 r(t) \tag{A.7}$$

with $r(t) < L/\Delta t$. Without such restriction, the recursively calculated values of i_0 used in Eq. (A.7) would generally lead to unstable solutions. At node n, the termination current is calculated according to

$$i_n = \frac{v_n}{R_t}. \tag{A.8}$$

The time step Δt should be at least an order of magnitude lower than the oscillation period of each line segment, $\tau \approx 2\pi\sqrt{LC}$, though $\Delta t \approx 0.01\tau$ or less will give more accurate results.

The above model is limited in that it does not include frequency-dependent variations of the distributed resistance, conductance or internal inductance of the line's conductors. Nonetheless, it is quite adaptable to simulate a number of other useful problems involving one-dimensional transmission lines.

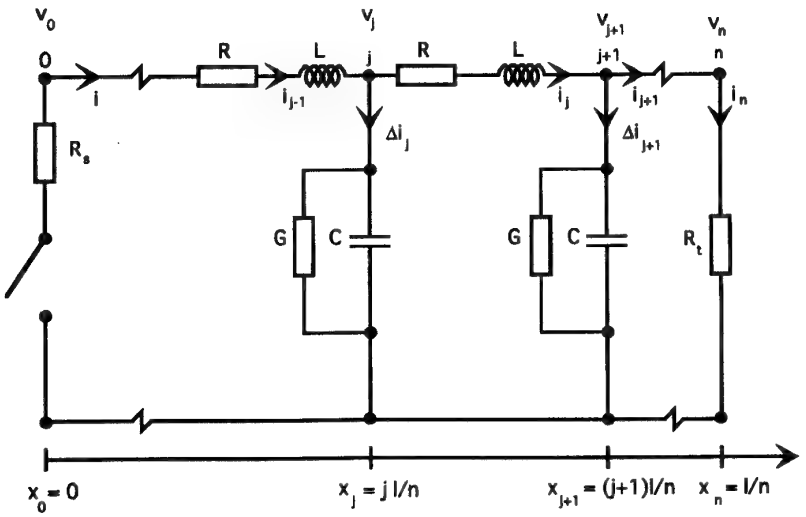

Figure A1: *Lumped circuit model of the finite transmission line problem with switch at node 0 and a high impedance termination at node n.*

Appendix B

Low Impedance Transmission Line Design

Our experimental requirements led us to design and build a low impedance, high current, high voltage transmission line. The required line impedance was of the order of 1Ω, so that current flows of the order of 1 kA or more could be generated at line voltage of 1 kV. The line also needed to withstand charge voltages of up to 5 kV. A simple parallel strip line design (e.g., References 14 and 15) was adopted, with a schematic cross-sectional view shown in Fig. B1. The nominal dimensions are: width of copper conductors, $w \cong 3.0\times10^{-2}$ m, thickness of kapton insulation and adhesive, $d \cong 1.25\times10^{-4}$ m. Although the relative permittivity of the adhesive is not known, we assume $\varepsilon_r \cong 3.3$ as that for the kapton film only. Since $w >> d$, then edge effects may be neglected and the formula for characteristic impedance [14,15] is

$$Z_0 = \frac{d}{w}\sqrt{\frac{\mu_0\mu_r}{\varepsilon_0\varepsilon_r}}, \qquad \text{(B.1)}$$

with $\mu_0 = 4\pi\times10^{-7}$ H/m, $\mu_r \approx 1$ and $\varepsilon_0 = 8.8542\times10^{-12}$ F/m. This gives a nominal value of $Z_0 \cong 0.86\,\Omega$, as required. The thickness of the copper conductors is nominally $d_c \cong 3.5\times10^{-5}$ m, which is approximately equal to one skin depth of annealed copper at current frequency of 3.5 MHz and temperature of 20°C.

The length of the strip line is governed by the desired duration of the switching event which was approximately 200 ns in our case. The maximum event window corresponds to the double transit time of a signal along the transmission line due to the line's finite length. Before the return of the reflected primary wave, generated by the switch closure, the line may be considered as semi-infinite, provided that dielectric leakage may be neglected. The transmission line constructed for our experiments was 33 m long and with a nominal velocity of signal propagation $c \cong 1.65\times10^{8}$ m/s, based on [14]

$$c = \frac{1}{\sqrt{\mu_0\mu_r\varepsilon_0\varepsilon_r}}. \qquad \text{(B.2)}$$

Hence the maximum expected event window was approximately 400 ns.

Since the transmission line was difficult to accommodate physically in its full length, it was wound helically onto a cardboard cylinder, approximately 0.5 m in diameter and 2 m in height. Generous lateral spacing of 0.05 m between windings was provided, which prevented electromagnetic coupling between windings as well as the possibility of accidental high voltage breakdown.

From the nominal values of the physical parameters supplied, the estimated strip line inductance per unit length is $L \cong 5.2$ nH/m and capacitance per unit length $C \cong 7.0$ nF/m, using [14]

$$L = \mu_0 \mu_r \frac{d}{w} \tag{B.3}$$

and

$$C = \varepsilon_0 \varepsilon_r \frac{w}{d} . \tag{B.4}$$

The resistance per unit length is estimated from the copper cross-section and resistivity. Since the resistive loss per unit length involves a series combination of the two transmission line conductors, then $R \cong 0.0328\ \Omega/\mathrm{m}$, using

$$R = \frac{2\rho_c}{dw} \tag{B.5}$$

with $\rho_c \cong 1.724 \times 10^{-8}\ \Omega$ m for annealed copper [21] at 20°C. Physical measurement of the total dc resistance of the line yielded $R \cong 0.0318\ \Omega/\mathrm{m}$. The frequency ($\omega$) dependent skin effect [14,15,21] is not included in Eq. (B.5) since it may be neglected for long signal duration, i.e., low frequencies, as well as high frequencies where the inductive component of line impedance, ωL, dominates the skin effect controlled resistive component, [14] $R \propto \sqrt{\omega}$.

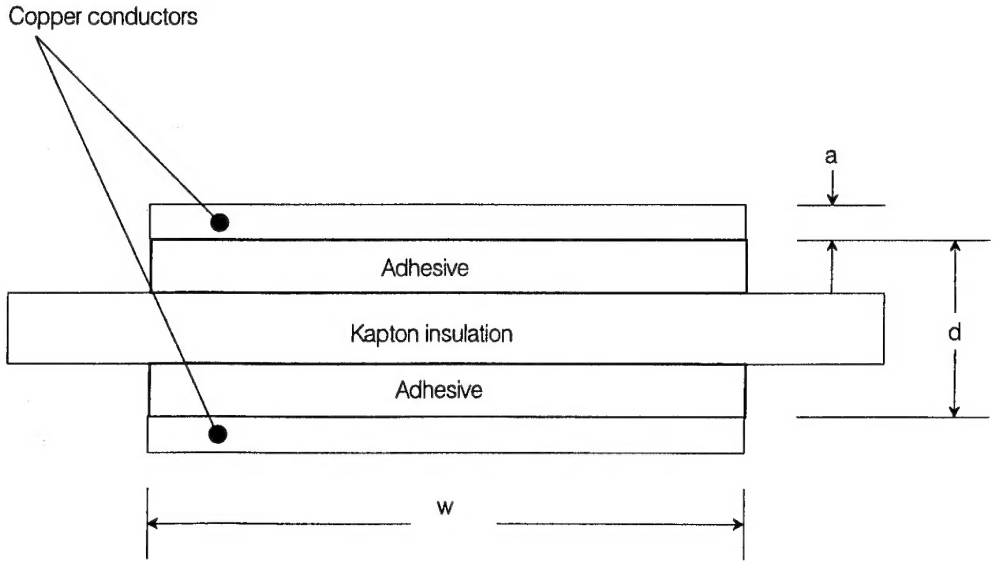

Figure B1: *Schematic cross-sectional view of parallel strip line employed in our experiments. "a" denotes the thickness of copper conductors, "d" the overall gap thickness between conductors and "w" the conductor width.*

Electrical Performance Characterisation of Single-Shot Switches in High Speed, High Voltage and High Current Applications

Michael Podlesak

(DSTO-RR-0010)

DISTRIBUTION LIST

Director, AMRL
Chief, Explosives Ordnance Division
Dr B.W. Thorpe
Dr M. Podlesak
Library, AMRL Maribyrnong
Library, AMRL Fishermens Bend

Chief Defence Scientist (for CDS, FASSP, ASSCM) 1 copy only
Director, ESRL
Head, Information Centre, Defence Intelligence Organisation
OIC Technical Reports Centre, Defence Central Library
Officer in Charge, Document Exchange Centre 7 copies
Senior Scientific Adviser
Air Force Scientific Adviser, Russell Offices
Scientific Adviser - Policy and Command
Senior Librarian, Main Library DSTOS
Librarian, DSD, Kingston ACT
Serials Section (M List), Deakin University Library, Deakin University, Geelong 3217
NAPOC QWG Engineer NBCD c/- DENGRS-A, HQ Engineer Centre, Liverpool Military Area, NSW 2174
ABCA, Russell Offices, Canberra ACT 2600 4 copies
Librarian, Australian Defence Force Academy
Head of Staff, British Defence Research and Supply Staff (Australia)
NASA Senior Scientific Representative in Australia
INSPEC: Acquisitions Section Institution of Electrical Engineers
Head Librarian, Australian Nuclear Science and Technology Organisation
Senior Librarian, Hargrave Library, Monash University
Library - Exchange Desk, National Institute of Standards and Technology, US
Acquisition Unit (DSC-EO/GO), British Library, Boston Spa, Wetherby, Yorkshire LS23 7BQ, England
Library, Chemical Abstracts Reference Service
Engineering Societies Library, US
Documents Librarian, The Center for Research Libraries, US
Army Scientific Adviser, Russell Offices - data sheet only
Navy Scientific Adviser - data sheet only
Director General Force Development (Land) - data sheet only
DASD, APW2-1-OA2, Anzac Park West, Canberra ACT - data sheet only
SO (Science), HQ 1 Division, Milpo, Enoggera, Qld 4057 - data sheet only
Librarian - AMRL Sydney - data sheet only
Counsellor, Defence Science, Embassy of Australia - data sheet only
Counsellor, Defence Science, Australian High Commission - data sheet only
Scientific Adviser to DSTC Malaysia, c/- Defence Adviser - data sheet only
Scientific Adviser to MRDC Thailand, c/- Defence Attache - data sheet only

John Waschl, EOD
Willard Hemsing, Los Alamos National Laboratory, USA
D.G. Tasker, Naval Surface Warfare Center, R13, Dahlgren, Virginia 22448-5000, USA
R.J. Lee, Naval Surface Warfare Center, R13, Dahlgren, Virginia 22448-5000, USA
P.K. Gustavson, Naval Surface Warfare Center, R13, Dahlgren, Virginia 22448-5000, USA

SECURITY CLASSIFICATION OF THIS PAGE **UNCLASSIFIED**

REPORT NO.	AR NO.	REPORT SECURITY CLASSIFICATION
DSTO-RR-0010	AR-008-582	Unclassified

TITLE

Electrical performance characterisation of single-shot switches in high speed, high voltage and high current applications

AUTHOR(S)
Michael Podlesak

CORPORATE AUTHOR
DSTO Aeronautical and Maritime Research Laboratory
GPO Box 4331
Melbourne Victoria 3001

REPORT DATE	TASK NO.	SPONSOR
August 1994	ARM 89/039	Army

FILE NO.	REFERENCES	PAGES
G6/4/8-4371	21	47

CLASSIFICATION/LIMITATION REVIEW DATE

CLASSIFICATION/RELEASE AUTHORITY
Chief, Explosives Ordnance Division

SECONDARY DISTRIBUTION

Approved for public release

ANNOUNCEMENT

Announcement of this report is unlimited

KEYWORDS

Electrical switches	Current measurement	Voltage measurement
Switch resistance	Waveforms	Transmission line

ABSTRACT

The electrical performance characteristics of single-shot closing switches for slapper detonator applications were measured via the discharge of a low impedance transmission line. The switch performance, characterised by its time-dependent resistance behaviour, could not be assessed via the more conventional methods of measurement because of high bandwidth requirements at comparatively high levels of voltage and current. Hence, an alternative technique based on a transmission line discharge was devised in which the time-dependent resistance of the switch can be determined from the measured current waveform of the switch, the initial open circuit voltage and the transmission line parameters only. Under certain conditions a simple lossless transmission line formula is sufficient for the calculation of the switch resistance waveform. However, if the transmission line losses cannot be neglected, a correction can be readily implemented through numerical signal processing. The bandwidth of this technique is limited to the bandwidth of the switch current measurement only, which proved to be particularly useful for the measurement of switches for slapper detonator applications where inductive pick-up noise in the switch voltage waveform is large and where high voltage probes of sufficiently high bandwidth are not readily available. In this report, both numerically simulated and experimental examples are given, together with the method of calculation of switch resistance which takes into account practical transmission line losses. It was found that best results are obtained if the magnitude of the switch resistance is of a similar order as the characteristic impedance of the transmission line, or higher.